Dalton Transactions

ROYAL SOCIETY OF CHEMISTRY

PERSPECTIVE

View Article Online
View Journal | View Issue

Cite this: *Dalton Trans.*, 2023, **52**, 17623

Thiol and thioether-based metal–organic frameworks: synthesis, structure, and multifaceted applications

Rajesh Patra, Sumit Mondal and Debajit Sarma *

Received 4th September 2023,
Accepted 31st October 2023

DOI: 10.1039/d3dt02884d

rsc.li/dalton

Metal–organic frameworks (MOFs) are unique hybrid porous materials formed by combining metal ions or clusters with organic ligands. Thiol and thioether-based MOFs belong to a specific category of MOFs where one or many thiols or thioether groups are present in organic linkers. Depending on the linkers, thiol-thioether MOFs can be divided into three categories: (i) MOFs where both thiol or thioether groups are part of the carboxylic acid ligands, (ii) MOFs where only thiol or thioether groups are present in the organic linker, and (iii) MOFs where both thiol or thioether groups are part of azolate-containing linkers. MOFs containing thiol-thioether-based acid ligands are synthesized through two primary approaches; one is by utilizing thiol and thioether-based carboxylic acid ligands where the bonding pattern of ligands with metal ions plays a vital role in MOF formation (HSAB principle). MOFs synthesized by this approach can be structurally differentiated into two categories: structures without common structural motifs and structures with common structural motifs (related to UiO-66, UiO-67, UiO-68, MIL-53, NU-1100, *etc.*). The second approach to synthesize thiol and thioether-based MOFs is indirect methods, where thiol or thioether functionality is introduced in MOFs by techniques like post-synthetic modifications (PSM), post-synthetic exchange (PSE) and by forming composite materials. Generally, MOFs containing only thiol-thioether-based ligands are synthesized by interfacial assisted synthesis, forming two-dimensional sheet frameworks, and show significantly high conductivity. A limited study has been done on MOFs containing thiol-thioether-based azolate ligands where both nitrogen- and sulfur-containing functionality are present in the MOF frameworks. These materials exhibit intriguing properties stemming from the interplay between metal centres, organic ligands, and sulfur functionality. As a result, they offer great potential for multifaceted applications, ranging from catalysis, sensing, and conductivity, to adsorption. This perspective is organised through an introduction, schematic representations, and tabular data of the reported thiol and thioether MOFs and concluded with future directions.

1. Introduction

Crystalline and porous compounds formed by the coordination interaction between metal ions or clusters with organic ligands are called metal–organic frameworks (MOFs).[1–5] From the time of their discovery in the 1990s, MOFs have received the utmost attention because of their extensive potential applications in fields like gas adsorption and separation,[6,7] heavy metal adsorption,[8,9] catalysis,[10–15] sensing,[16–18] drug delivery,[19,20] electrical conductivity,[21] proton conductivity,[22] photocatalysis,[23] materials with magnetic properties,[24,25] and optical devices[26,27] *etc*. The root cause of their diverse applications is excellent stability,[28] high surface areas,[29] ordered porosity[30] and fascinating tuneable functionalities.[31] To achieve specific physical and chemical characteristics, researchers have dedicated considerable effort to the development of stable metal–organic frameworks (MOFs), including distinct organic ligands with convertible functionalities *viz*., $-NH_2$,[32] –OH,[33] –X (halogen),[34] –R (alkyl),[35] –SH and –SR,[36] *etc*. The presence of thiol (–SH) and thioether (–SR) groups in MOFs added an extra feature that increases the reactivity and selectivity of the pristine MOFs.[37] Thiol and thioether groups have a unique feature as they are electronically soft and easily polarisable, making thiol and thioether-based MOF useful for potential applications.[37]

Li *et al.* have reviewed the adsorption application of thiol and thioether-based MOFs, and Deng *et al.* have reviewed the conductivity of some of the thiol MOFs.[38,39] Unfortunately, no perspective or comprehensive review encompasses the entirety of thiol and thioether-based MOFs with synthesis, structural analysis and applications. This perspective summarises the thiol and thioether-based MOF syntheses, structures, and their multifaceted spectrum of applications in tabular and sche-

Department of Chemistry, Indian Institute of Technology Patna, Bihar 801106, India. E-mail: debajit@iitp.ac.in, rajesh_1921ch07@iitp.ac.in, sumit_1921ch12@iitp.ac.in

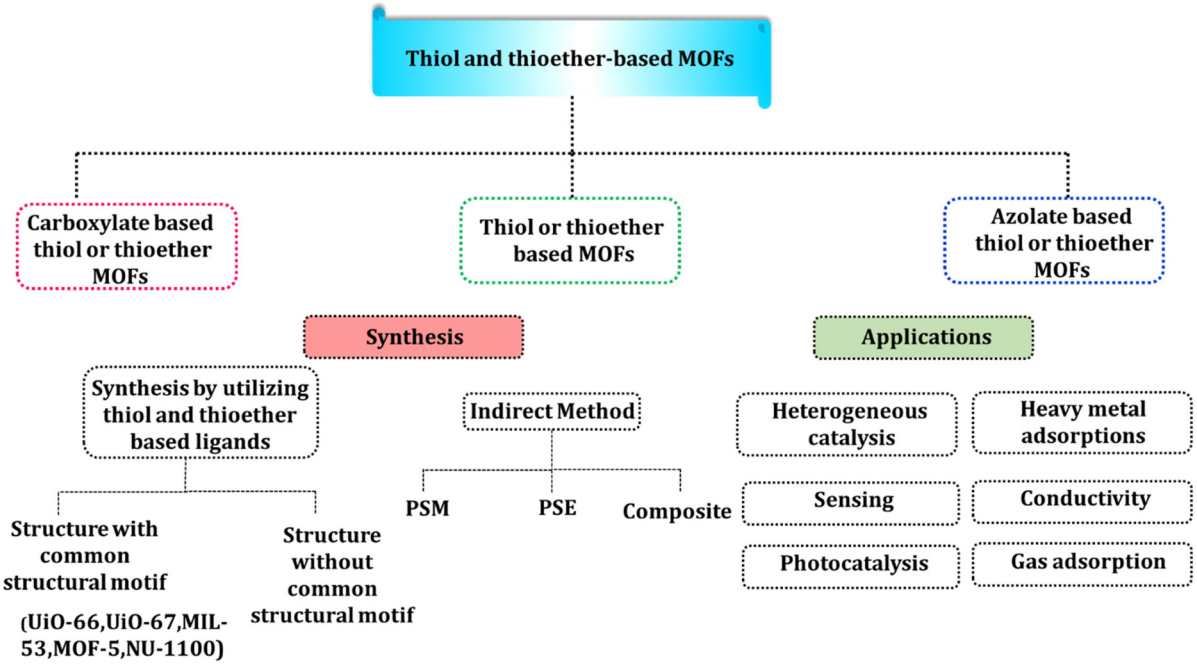

Fig. 1 Schematic overview of thiol and thioether-based MOFs. (PSM: post-synthetic modifications, and PSE: post-synthetic exchange.)

matic form. Finally, this perspective is summarized with limitations and future aspects of the thiol and thioether-based MOFs (Fig. 1).

2. Thiol and thioether-based MOFs: an overview

2.1 Chemistry of thiol and thioether functional groups

Thiols (–SH) and thioethers (–SR) are important functional groups containing sulfur atoms that exhibit fascinating reactivity and play significant roles in various biological, chemical, industrial, and environmental processes.[40,41] In thiols, the sulfur-hydrogen bond is polar, which makes it reactive. Thiols are integral components of living systems, playing vital roles in maintaining cellular health and functioning.[42] Glutathione, a tripeptide composed of three amino acids (cysteine, glycine, and glutamic acid), is a prime example of a thiol-based molecule with significant biological importance.[43] Glutathione acts as a potent antioxidant, scavenging harmful reactive oxygen species and protecting cells from oxidative stress.[44] Thiols also find applications in various industrial and synthetic processes beyond their biological role.[45] Thiols are notable for their nucleophilic behaviour, participating in nucleophilic substitution, addition, and redox reactions.[46] They find use in the production of sulfur-containing chemicals like thiourea and mercaptobenzothiazole, as well as in the synthesis of pharmaceuticals and agrochemicals.[47] In organic synthesis, thiols are


Rajesh Patra

Rajesh Patra was born in Bankura, West Bengal, India. He obtained his B.Sc. (Honours) degree in Chemistry from Burdwan University, and M.Sc. from Pondicherry University, India, in Chemical Science. Currently, he is working on thiol-based MOFs and their catalytic applications with the Solid-State and Inorganic Chemistry Group at the Indian Institute of Technology, Patna.


Sumit Mondal

Sumit Mondal was born in Burdwan, West Bengal, India. He obtained his B.Sc. (Honours) degree in Chemistry from Burdwan University, India. His M.Sc. degree was completed in Organic Chemistry from Bilaspur University, Chhattisgarh, India. Recently he has been working in the field of porous material synthesis and its application in catalysis and sensing with the Solid-State and Inorganic Chemistry Group at the Indian Institute of Technology, Patna.

utilized in thiol–ene reactions, which have implications in fields ranging from materials science to drug discovery.[48,49]

Thioethers feature a sulfur atom bonded to two organic groups.[50] This structural arrangement imparts distinctive properties to thioethers, making them essential in various chemical transformations. Thioethers are crucial in stabilizing protein structures and act as structural anchors, maintaining protein conformation.[51] Furthermore, they are often employed as protecting groups in organic synthesis, facilitating selective reactions while shielding sensitive functional groups.[52] In inorganic chemistry, thioethers serve as ligands in coordination complexes, aiding in the design of novel catalysts and materials.[53]

The synthesis of thiols and thioethers has been a focal point of research due to their importance in diverse fields. Classical methods for thiol synthesis include nucleophilic substitution reactions involving halides or sulfonates with thiolate ions and the reduction of disulfides.[54] Thioethers are commonly synthesized *via* nucleophilic substitution or metal-catalyzed coupling reactions.[55] Despite their importance, thiol and thioether chemistry also presents challenges.[56] Thiol oxidation, leading to the formation of disulfide bonds, can impact protein structure and function, causing disease.[57] Developing selective thiol and thioether functionalization methods remains an ongoing challenge in synthetic chemistry. In addition, the comprehensive understanding of the complex relationship between sulfur-containing compounds and biological systems demands collaborative endeavours across chemistry, biology, and medicine disciplines.[58]

2.2 Thiol and thioether-based MOFs

Metal–organic frameworks (MOFs) elegantly merge metal salts with organic linkers or ligands.[59] Depending on the linkers, thiol-thioether MOFs can be divided into three categories (Fig. 2): (i) MOFs where both thiol or thioether groups are present in carboxylic acid-containing ligands, (ii) MOFs where only thiol or thioether groups are present in the organic linker, and (iii) MOFs where both thiol or thioether groups are part of azolate-containing linkers.

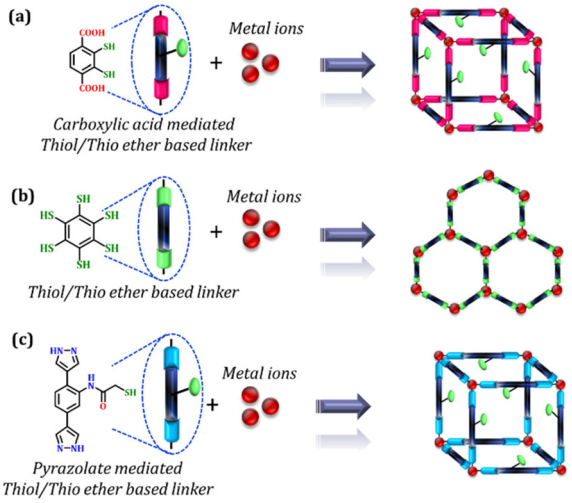

Fig. 2 Schematic represent of different kind of thiol-thioether-based MOF (a). MOFs where both thiol or thioether groups are present in carboxylic acid-containing ligands. (b) MOFs where only thiol or thioether groups are present in the organic linker. (c) MOFs where both thiol or thioether groups are part of azolate-containing linkers.

Among these thiol or thioether-based ligands, those housing carboxylic groups stand out as exceptionally advantageous in synthesising MOFs.[5] As the exploration of MOFs has progressed, the landscape has broadened beyond solely relying on carboxylic acid ligands.[60,61] A rich array of alternative ligands, enriched with carboxylic acid groups, in conjunction with supplementary functional moieties (such as –R (alkyl), $–NH_2$, –OH, and –X (halogen)) have gained substantial attention due to their remarkable stability, fine-tunability, and distinctive applications spanning a multitude of domains.[33–35,62] In these functional group categories, MOFs with organic ligands containing thiol (–SH) and thioether (–SR) functional groups are called thiol and thioether-based MOFs.[63–65] There are cases when the thiol-thioether functional groups are installed in pre-synthesized MOFs by the organic transformation of other functional groups containing MOFs by post-synthetic treatment, which are also considered thiol and thioether-based MOFs.[66] The combination of hard and soft functional groups in the MOF framework makes thiol and thioether-based MOFs stand out as unique in the category of functional MOFs. Owing to these exceptional attributes, thiol and thioether-based MOFs find extensive utility across a diverse spectrum of applications, encompassing catalysis, sensing, adsorption, and conductivity.[67–70] In case of linkers where only thiol or thioether groups are present, the MOFs are generally synthesized by inert atmosphere interfacial assisted methods as these ligands are air and moisture sensitive.[71,72] MOFs of this category are well-known for their unique two-dimensional (2D) sheet structures, which are responsible for their high conductive nature.[73] Synthesis of MOFs with both sulfur and nitrogen functionality is a challenging task, and for

Debajit Sarma

Debajit Sarma received his M.Sc. from the Indian Institute of Technology, Delhi, and Ph.D. from the Indian Institute of Science, Bangalore. After working as a Postdoctoral Fellow at Northwestern University, he joined as an Assistant Professor in the Department of Chemistry at the Indian Institute of Technology, Patna, in 2017. His current research interests include inorganic materials for sensing, catalysis, energy conversion, and environmental remediation.

that reason, only a few reports are available for MOFs containing thiol-thioether-based azolate ligands.[74–76]

3. Synthesis and structure of thiol and thioether-based-acid ligands containing MOFs

In general, there are two common ways to synthesize thiol and thioether-based-acid ligands containing MOFs: (i) synthesis by utilizing thiol or thioether-based-acid ligands, and (ii) indirect synthesis involving the strategic incorporation of thiol or thioether groups to a parent MOF through a spectrum of diverse techniques, including post-synthetic modifications (PSM), post-synthetic exchange (PSE), mixed ligand strategies and composite formulations. The pursuit of thiol and thioether-based ligands for synthesizing their corresponding MOFs has captivated considerable attention owing to its elegantly simple nature. However, owing to the inherent versatility of the indirect approach, it emerges as a valuable and advantageous method for synthesizing thiol and thioether-based MOFs. MOF composite materials are necessary for practical uses. Structurally, thiol and thioether-based acid ligand-containing MOFs can be broadly differentiated into two categories: (i) thiol and thioether-based MOFs without common structural motifs and (ii) structures with common structural motifs, when the structure of MOFs is isoreticular with well-established MOFs like UiO-66, UiO-67, UiO-68, MIL-53, MOF-5, *etc*.[77–79]

3.1 Synthesis by utilizing thiol or thioether-based acid ligands

The solvothermal process is a widely used method for synthesizing MOFs.[80] Generally, by solvothermal methods, thiol or thioether-containing ligands (Fig. 3 and 4) react with metal salts to form the corresponding MOFs. The ligands contain two electronically different functional groups: one is the electronically hard carboxylic acids group, and the other one is the electronically soft thiol or thioether group. As two distinct functional groups are present in the organic linker, the ligand and metal ion connectivity follows HSAB principles. The electronically hard acids groups tend to form a bond with hard metal ions like Zr^{4+}, Fe^{3+}, In^{3+}, Al^{3+}, Cu^{2+}, Zn^{2+}, and Co^{2+}, and electronically soft thiols or thioethers remain as free-standing groups.[81,82] On the other hand, electronically soft thiol and thioether functional groups tend to bind with soft metal ions like Cu^{+}, Ag^{+}, Cd^{2+}, Mn^{2+}, and carboxylic acids groups remain free-standing groups.[83]

3.1.1 Thiol and thioether MOFs without common structural motifs

3.1.1.1 Thiol MOFs without common structural motifs. The solvothermal reaction between the metal salt and the corresponding thiol ligand directly synthesizes thiol-based MOFs. Thiol MOFs, which show structures without any specific common structural motif, are listed in Table 1. Initial reports of thiol-containing MOFs were with the thiol-based ligand L_1 (H_2DMBD), reported in 2009 by He *et al.*[65] In the report, different bonding patterns (according to the HSAB principle) of the thiol-based ligand H_2DMBD with metal ions such as

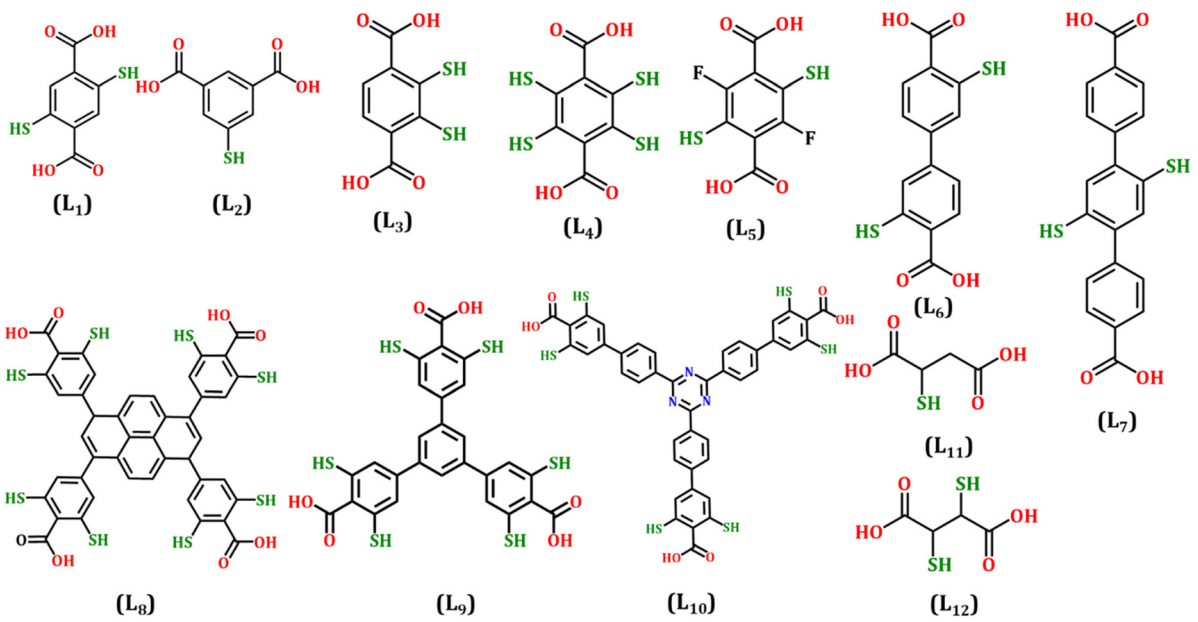

Fig. 3 (L_1) 2,5-Dimercaptoterephthalic acid, (L_2) 5-mercaptoisophthalic acid, (L_3) 2,3-dimercaptoterephthalic acid, (L_4) 2,3,5,6-tetramercaptoterephthalic acid, (L_5) 2,5-difluoro-3,6-dimercaptoterephthalic acid, (L_6) 3,3′-dimercapto-1,1′-biphenyl-4,4′-dicarboxylic acid, (L_7) 2′,5′-dimercapto-1,1′:4′,1″-terphenyl-4,4″-dicarboxylic acid, (L_8) 4,4′,4″,4‴-(1,6-dihydropyrene-1,3,6,8-tetrayl)tetrakis(2,6-dimercaptobenzoic acid), (L_9) 5′-(4-carboxy-3,5-dimercaptophenyl)-3,3″,5,5″-tetramercapto-[1,1′:3′,1″-terphenyl]-4,4″-dicarboxylic acid, (L_{10}) 4′,4‴,4⁗″-(1,3,5-triazine-2,4,6-triyl)tris (3,5-dimercapto-[1,1′-biphenyl]-4-carboxylic acid), (L_{11}) 2-mercaptosuccinic acid, (L_{12}) 2,3-dimercaptosuccinic acid.

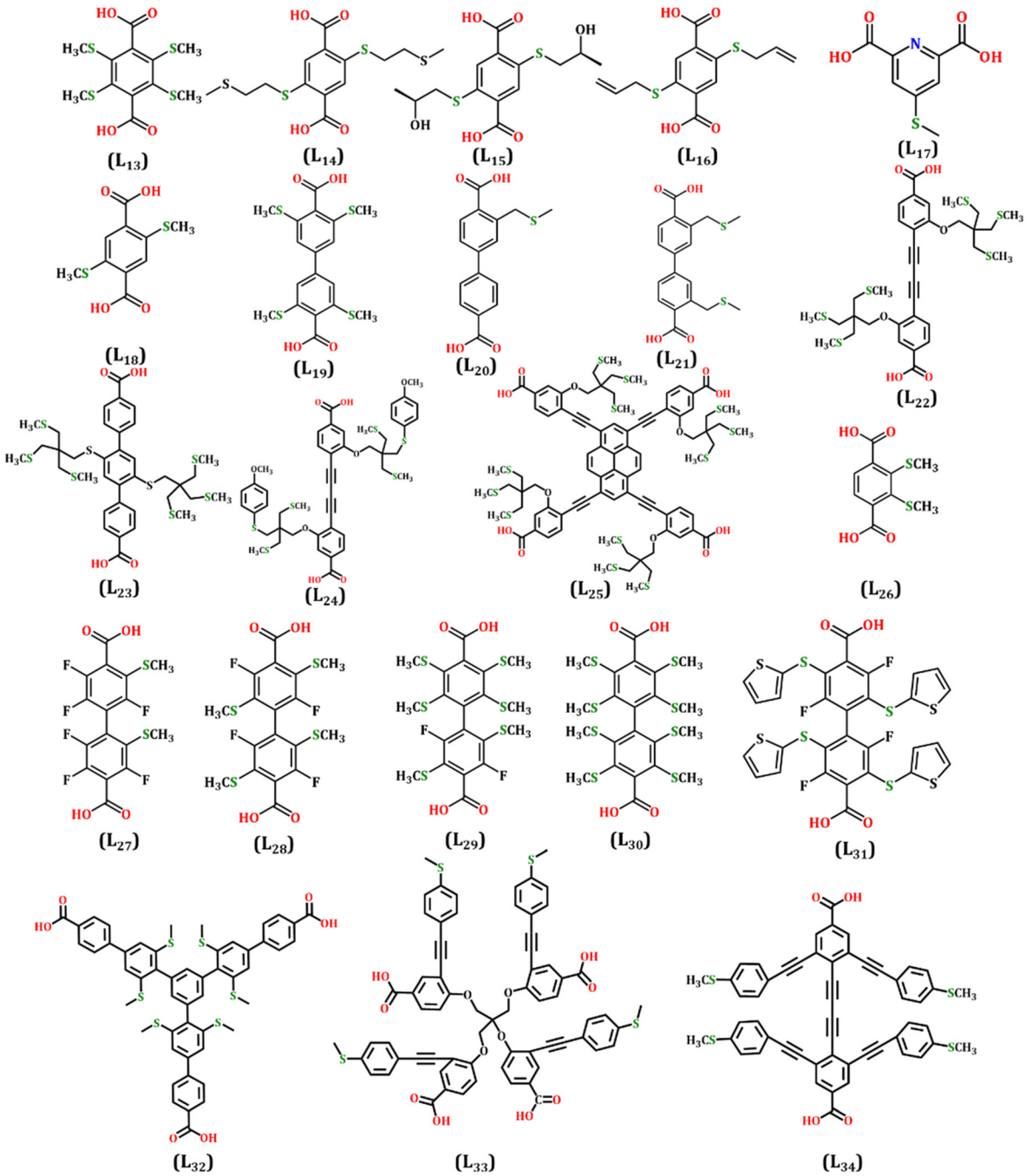

Fig. 4 (L_{13}) 2,3,5,6-Tetrakis(methylthio)terephthalic acid, (L_{14}) 2,5-bis(2(methylthio)ethylthio)terephthalic acid, (L_{15}) 2,5-bis(((*S*)-2-hydroxypropyl)thio)terephthalic acid, (L_{16}) 2,5-bis(allylthio)terephthalic acid, (L_{17}) 4-(methylthio)pyridine-2,6-dicarboxylic acid, (L_{18}) 2,5-bis(methylthio)terephthalic acid, (L_{19}) 3,3′,5,5′-tetrakis(methylthio)-[1,1′-biphenyl]-4,4′-dicarboxylic acid, (L_{20}) 3-((methylthio)methyl)-[1,1′-biphenyl]-4,4′-dicarboxylic acid, (L_{21}) 3,3′-bis((methylthio)methyl)-[1,1′-biphenyl]-4,4′-dicarboxylic acid, (L_{22}) 4,4′-(buta-1,3-diyne-1,4-diyl)bis(3-(3-(methylthio)-2,2-bis((methylthio)methyl)propoxy)benzoic acid), (L_{23}) 2′,5′-bis((3-(methylthio)-2,2-bis((methylthio)methyl)propyl)thio)-[1,1′:4′,1″-terphenyl]-4,4″-dicarboxylic acid, (L_{24}) 4,4′-(buta-1,3-diyne-1,4-diyl)bis(3-(3-((4-methoxyphenyl)thio)-2,2-bis((methylthio)methyl)propoxy)benzoic acid), (L_{25}) 4,4′,4″,4‴-(pyrene-1,3,6,8-tetrayltetrakis(ethyne-2,1-diyl))tetrakis(3-(3-(methylthio)-2,2-bis((methylthio)methyl)propoxy)benzoic acid), (L_{26}) 2,3-bis(methylthio)terephthalic acid, (L_{27}) 2,2′,3,3′,5,6′-hexafluoro-5′,6-bis(methylthio)-[1,1′-biphenyl]-4,4′-dicarboxylic acid, (L_{28}) 2,2′,5,5′-tetrafluoro-3,3′,6,6′-tetrakis(methylthio)-[1,1′-biphenyl]-4,4′-dicarboxylic acid, (L_{29}) 2,5-difluoro-2′,3,3′,5′,6,6′-hexakis(methylthio)-[1,1′-biphenyl]-4,4′-dicarboxylic acid, (L_{30}) 2,2′,3,3′,5,5′,6,6′-octakis(methylthio)-[1,1′-biphenyl]-4,4′-dicarboxylic acid, (L_{31}) 2,2′,5,5′-tetrafluoro-3,3′,6,6′-tetrakis(thiophen-2-ylthio)-[1,1′-biphenyl]-4,4′-dicarboxylic acid, (L_{32}) 5″-(4′-carboxy-3,5-bis(methylthio)-[1,1′-biphenyl]-4-yl)-2‴,3′,5′,6‴-tetrakis(methylthio)-[1,1′:4′,1″:3″,1‴:4‴,1⁗-quinquephenyl]-4,4⁗-dicarboxylic acid, (L_{33}) 4,4′,4″-((2-((4-carboxy-2-((4-(methylthio)phenyl)ethynyl)phenoxy)methyl)propane-1,2,3-triyl)tris(oxy))tris(3-((4-(methylthio)phenyl)ethynyl)benzoic acid), (L_{34}) 4,4′-(buta-1,3-diyne-1,4-diyl)bis(3,5-bis((4-(methylthio)phenyl)ethynyl)benzoic acid.

Table 1 Thiol MOFs without common structural motifs

Entry no.	Molecular formula	Ligand	Synthetic methodology	Dimensionality	BET surface area (m^2 g^{-1})	Applications	Ref.
1	$Cu_6(DMBD)_3(en)_4(Hen)_6$	2,5-Dimercapto-1,4-benzenedicarboxylic acid (H_2DMBD)	Solvothermal	2D	—	—	65
2	$Pb_2(DMBD)(en)_2$	(L_1)		2D	—		
3	$Eu_2(H_2DMBD)_3(DEF)_4$			3D	—		
4	$Eu(DFDMT)_2$	2,5-Difluoro-3,6-dimercaptoterephthalate acid (H_2DFDMT) (L_5)	Solvothermal	2D		Conductivity	70
5	$[((CH_3)_2NH_2)Cd(MIPA)]_4{\cdot}xG$	5-Mercaptoisophthalic acid (H_3MIPA) (L_2)	Solvothermal	3D	2169	Dye separation	83
6	$[((CH_3)_2NH_2)Cd(MIPA)]_2{\cdot}xG$			3D	2236		
7	$[((CH_3)_2NH_2)Cd(MIPA)]_1{\cdot}xG$			3D	2295		

Cu^+, Pb^{2+}, and Eu^{3+} (Table 1, entry no. 1–3) of varying hardness (hardness $Cu^+ < Pb^{2+} < Eu^{3+}$) were explained. In the reactions when the ligand H_2DMBD reacts with softer Cu^+ and forms a coordination network, only the thiol group of the ligand bonded with the metal, and the carboxylic acid group remains as a free-standing group (Fig. 5a). However, in the case of moderately hard Pb^{2+}, both the functional groups of the ligand are bonded with the metal ion (Fig. 5b). Eu^{3+}, a hard metal ion, only allows the carboxylic group to attach to the metal ion, and the thiol group remains free-standing (Fig. 5c). Although the Eu metal and H_2DMBD-containing MOF do not show special applications due to the absence of a stable porous site, this bonding pattern concept opens up various routes for synthesizing different thiol-based MOFs. Interestingly, in contrast to the common idea of the bonding pattern of thiol-based MOFs $Eu(DFDMT)_2$ synthesized by the combination of fluorine-containing thiol-based ligand L_5 (H_2DFDMT) and $EuCl_3{\cdot}6H_2O$ leads to a 2D structure (Table 1, entry no. 4) where sulfur is bonded with Eu^{3+} (Fig. 5d).[70]

The Eu MOF shows moderate conductivity due to extended metal thiolate π bonding. Dong *et al.* reported three different variants of thiol-containing MOF $[((CH_3)_2NH_2)Cd(MIPA)]_n{\cdot}xG$ (n = 4 (compound **1**), 2 (compound **2**), 1 (compound **3**); G = guest of DMF/DMA and H_2O), from the combination of ligand L_2 (H_3MIPA) and $Cd(NO_3)_2{\cdot}4H_2O$ under solvothermal conditions at 150–160 °C for 3 days.[83] Three different ratios of the solvent [DMA/H_2O = 4 : 1 for compound **1**, DMF/H_2O = 3 : 2 for compound **2**, and DMA/H_2O = 2 : 3 for 3] lead to three different compounds (Table 1, entry no. 5–7). The ligand $[MIPA]^{3-}$ in all the compounds connected with the Cd^{2+} centres by a μ^4-bridge, where two carboxylate groups exhibit the same μ^1–η^1:η^1

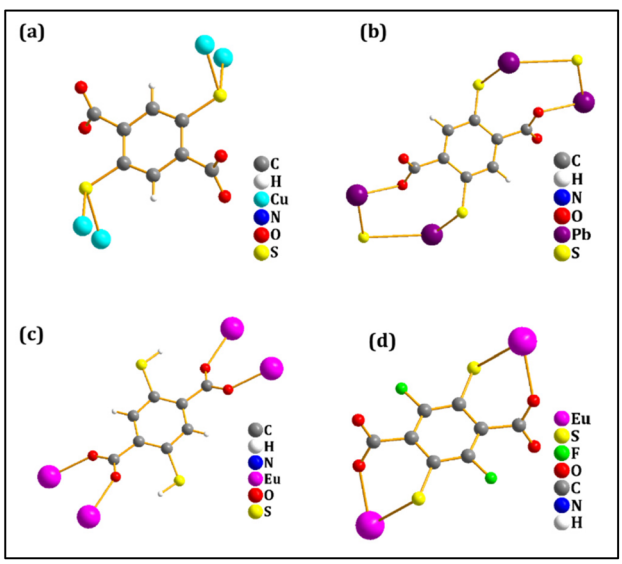

Fig. 5 Structure of (a) $Cu_6(DMBD)_3(en)_4(Hen)_6$, (b) $Pb_2(DMBD)(en)_2$, (c) $Eu_2(H_2DMBD)_3(DEF)_4$,[65] (d) $Eu(DFDMT)_2$.[70] (Drawn from CIF files 713331, 713332, 713333, and 1941723 with permission from Elsevier Inc and the Royal Society of Chemistry.)

chelate coordination mode and the mercapto group connected through a μ^2 coordination mode.

3.1.1.2 Thioether MOFs without common structural motifs. Like thiol-based MOFs, many new thioether-based MOFs have been synthesized by solvothermal or hydrothermal methods, listed in Table 2. Zhou *et al.* did the initial study on thioether-based MOF in 2008 using the ligand L_{13} (TMBD).[84] The ligand TMBD contains two different functional groups: electronically hard carboxyl (–COOH) and soft methyl-thio ($-SCH_3$). The first report showed the bonding pattern of the synthesized MOFs Cu_2TMBD, CdTMBD (Table 2, entry no. 1 and 2) and $Zn_4O(H_2O)_3$(TMBD)$_3$ (Table 5, entry no. 1) with metal ions of different hardness. The hardness of the metal ions Cu^+, Cd^{2+}, and Zn^{2+} is 6.3, 10.3, and 10.8 (ηA), respectively (HASB-principle), where the carboxyl group binds with harder metal ions to form the coordination networks while the softer methyl-thio group binds with softer metal ions. The three MOFs show three different bonding patterns. As for different MOFs, the S atoms of the methyl-thio group bonded differently, like bonded sulfur with Cu^+ in Cu_2TMBD (Fig. 6a), half of the sulfur bonding to Cd^{2+} in CdTMBD (Fig. 6b), and nonbonding sulfur in $Zn_4O(H_2O)_3$(TMBD)$_3$. In the crystal of Cu_2TMBD and CdTMBD, the methyl-thio group is bonded with the metal ion, so no substantial porosity is observed, but in the case of $Zn_4O(H_2O)_3$(TMBD)$_3$, as the methyl-thio groups of the TMBD ligand do not coordinate with the metal ion Zn^{2+} reasonable porosity is reported. The extension of this study was reported in 2010 by the same group, where three different coordination networks are formed by simple hydrothermal synthesis and varying the ratio of the metal salt $Cu(NO_3)_2$ and the ligand TMDB (Table 2, entry no. 3 and 4).[85] A relatively small (1 : 1) $Cu(NO_3)_2$/TMBD ratio formed $Cu(TMBD)_{0.5}(H_2TMBD)_{0.5}$ $3H_2$TMBD and crystallizes as a one-dimensional (1D) coordination assembly based on Cu^+-thioether interactions, which is integrated by hydrogen bonding to additional H_2TMBD molecules to form a three-dimensional (3D) supramolecular network with all the carboxylic acid and carboxylate groups remaining uncoordinated. When the ratio of metal salt increases from 1 : 1 to 1.25 : 1 [$Cu(NO_3)_2$/TMBD (1.25 : 1)], initially reported Cu_2TMBD is observed where the metal ion Cu^+ bonds with both the carboxylate and thioether groups. Again, enhancement of the metal ratio [$Cu(NO_3)_2$/TMBD (2.4 : 1)] leads to a unique mixed-cation compound $Cu^{II}_2OHCu^{I}$ $(TMBD)_2{\cdot}2H_2O$ where the carboxylic groups are bonded to Cu^{2+} ions, while the thioether groups bonded to Cu^+. In 2018, Liu *et al.* published an interesting report where they used water as a solvent with the same ligand and a different Cu salt (Table 2, entry no. 5).[86] The serendipity occurs while synthesizing Cu_2TMBD-np, and after analyzing and changing the metal salt from $Cu(NO_3)_2$ to $(CH_3CN)_4BF_4$, a new MOF (CityU-7) was formed in the solvothermal process where Cu^+ ions are simultaneously bonded with carboxyl and thioether in the crystal structure (Fig. 6c). The same group also synthesized Pb-TMBD by the solvothermal reaction between $Pb(NO_3)_2$ and TMBD in DMA-acetonitrile solvent (Table 2, entry no. 6).[87] The crystal study reveals that Pb-TMBD forms a 3D structure where some

Table 2 Thioether MOFs without common structural motifs

Entry no.	Acronym name	Molecular formula	Ligand	Synthetic methodology	Dimensionality	BET surface area (m^2 g^{-1})	Application	Ref.
1	Cu-TMBD	$Cu(TMBD)_{0.5}$	2,3,5,6–2,3,5,6-Tetrakis(methylthio)terephthalic acid (TMBD) (L_{13})	Hydrothermal	3D	—	Bonding of thioether ligand	84
2	Cd-TMBD	Cd(TMBD)		Solvothermal	3D	—		
3	—	$[Cu(TMBD)_{0.5}(H_2TMBD)_{0.5}\ 3H_2TMBD]$		Solvothermal	3D	—	NH_3 sensing	85
4	—	$Cu^{II}_2OH\ Cu^{I}\ (TMBD)_2{\cdot}2H_2O$		Solvothermal	3D	—		85
5	CityU-7	$Cu_2(C_{12}H_{12}S_4O_4)(H_2O)_2$		Solvothermal	3D	197	CO_2, water, and iodine uptake	86
6	PbTMBD	$Pb_3(TMBD)_3{\cdot}2DMA\ 0.79\ H_2O$		Solvothermal	3D	—	$HgCl_2$ uptake	87
7	Eu-MOF	$[Eu_4(OH)_4(H_2O)_4]_2{\cdot}(C_{12}H_{12}O_4S_4)_9$	4-(Methylthio)pyridine-2,6-dicarboxylic acid (L_{17})	Hydrothermal	3D	—	AgCl trapping	88
8	Cd-MOF	$C_8H_9CdNO_6S$	4′,4‴,4⁗-(1,3,5-Triazine-2,4,6-triyl)tris(3′,5′-bis (methylthio)-[1,1′-biphenyl]-4-carboxylic acid) (L_{32})	Hydrothermal	3D		Luminescence sensing	69
9	GDUT-7	$Eu{\cdot}L_{32}{\cdot}(DMF)_{3.5}{\cdot}(H_2O)_4$		Solvothermal	3D	—	Mercury and iodine removal	89
10	BFMOF-1	$Pb_6O_2(C_{69}H_{48}O_{12}S_4)_2(DMA)_3(H_2O)_2$	4,4′,4″-((2-((4-Carboxy-2-((4-(methylthio)phenyl) ethynyl)phenoxy)methyl)propane-1,2,3-triyl)tris (oxy))tris(3-((4-(methylthio)phenyl)ethynyl) benzoic acid) (L_{33})	Solvothermal	3D	318	Uptake of Lewis acid $PdCl_2$ and Lewis base H_2S	90
11	—	$\{Cu^{II}_4[(S,S)\text{-methox}]_2\}{\cdot}5H_2O$	Methox: [(*S*)-methionine]oxalyl diamide	Hydrothermal	3D		Mercury removal	91
12	—	$\{Ca^{II}Cu^{II}_5[(S,S)\text{-methox}]_3(OH)_2(H_2O)\}{\cdot}16H_2O$	Methox: [(*S*)-methionine]oxalyl diamide	Hydrothermal	3D	153	Catalysis	92 and 93
13	—	$\{Sr^{II}Cu^{II}_6[(S,S)\text{-serimox}]_{1.50}[(S,S)\text{-mecys-mox}]_{1.50}(OH)_2(H_2O)\}{\cdot}12H_2O$	Serimox = bis[(*S*)-serine]oxalyldiamide	Slow diffusion	3D		Catalysis	94

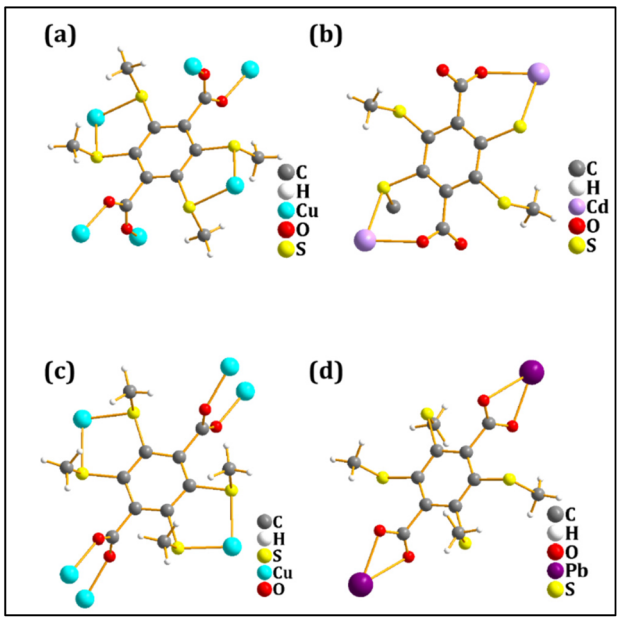

Fig. 6 (a) Local coordination environment of Cu_2TMBD, (b) local coordination environment of CdTMBD,[84] (c) local coordination environment of Cu(I) in CitU-7,[86] (d) crystal structure of Pb-TMBD.[87] (Drawn from CIF file with permission from the American Chemical Society and Royal Society of Chemistry.)

of the thioether groups remain free-standing (Fig. 6d), responsible for their application in $HgCl_2$ adsorption. Zhou *et al.* synthesized Eu MOF (Table 2, entry no. 7) with H_2TMBD; the thioether groups remain free-standing, stabilising soft guests like AgCl.[88] Recently, Mohan *et al.* synthesized a new thioether-based ligand L_{17} and its corresponding Cd MOF (Table 2, entry no. 8) by a solvothermal reaction with Cd $(NO_3)_2{\cdot}4H_2O$ in water solvent.[69] The colourless compound crystallized in the triclinic $R\bar{3}$ space group and formed a 3D coordination network with the free $-SCH_3$ group. This water- and pH-stable MOF acts as a luminescence sensor for heavy metals.

GDUT-7 (Table 2, entry no. 9) was synthesized by He *et al.* with L_{32}.[89] The compound was crystalized in the *C*2/*c* space group where the Eu centre is 8-coordinated, and the dimer formed by Eu is centrosymmetric. The overall structure of GDUT-7 is 3D with the non-interpenetrated (6,3) net. Amphoteric MOF, BFMOF-1 (Table 2, entry no. 10), was reported in 2014 by Cui *et al.* where L_{33} was used as a ligand, and the structure shows the coexistence of free-standing sulfur donors and labile-capped Pb(II) centres as accessible acceptor sites.[90] BFMOF-1 can effectively take up both Lewis acid (such as $PdCl_2$) and Lewis base (such as H_2S) guests. Pardo and co-workers utilized the thioether-based natural ligand L-methionine to synthesize chiral ligand H_2Me_2-(*S*,*S*)-methox. The ligand was utilized to a series of bioMOFs $\{Cu^{II}_4[(S,S)\text{-methox}]_2\}{\cdot}5H_2O$,[91] $\{Ca^{II}Cu^{II}_6[(S,S)\text{-methox}]_3(OH)_2(H_2O)\}{\cdot}16H_2O$,[92,93] and $\{Sr^{II}Cu^{II}_6[(S,S)\text{-serimox}]_{1.50}[(S,S)\text{-mecysmox}]_{1.50}(OH)_2(H_2O)\}{\cdot}12H_2O$,[88] with unique structural properties and applications (Table 2, entry no. 11–13).

3.1.2 Thiol and thioether-based MOFs with common structural motifs

3.1.2.1 Thiol-based MOFs with common structural motifs. Thiol-based MOFs with common structural motifs are listed in Table 3. On one side is the synthesis of Eu-MOF, where the electronically soft thiol group remains a free-standing group; on the other side, the development of the well-known UiO-66 MOF encouraged researchers to synthesize isoreticular thiol-based MOFs, where the thiol groups remain as free-standing groups.[65,77] Generally, UiO-66 is synthesized by the solvothermal reaction between zirconium tetrachloride salt ($ZrCl_4$) and terephthalic acid (H_2BDC) in *N*,*N*′-dimethylformamide (DMF) solvent.[95] Later, Wißmann *et al.* reported modulated synthesis using acetic acid (CH_3COOH) as a modulator where UiO-66 crystalizes in a face-centered-cubic (fcc) arrangement.[96] The crystal structure of UiO-66 contains $Zr_6O_4(OH)_4$ clusters with 12-connected nodes as SBU and 1,4-benzenedicarboxylate as an organic linker. Like UiO-66, isoreticular UiO-66$(SH)_2$ was reported in 2013 by Yee *et al.*, the most studied thiol MOF (Table 3, entry no. 1).[37] The synthetic procedure of UiO-66 $(SH)_2$ (abbreviated as Zr-DMBD) is similar to the synthesis of UiO-66 where the ligand L_1 (H_2DMBD) is used instead of terephthalic acid (H_2BDC) (Fig. 7a). The thiol group of the ligand remains a free-standing group in the MOF structure as only carboxylic acid groups bind with the Zr-cluster.

The valuable applications of Zr-DMBD are due to this free-standing thiol group; since it is very reactive and easily functionalizable, there are numerous opportunities for post-synthetic modifications for specific applications.[97–107] All reported post-synthetic modifications of Zr-DMBD for their significant applications are listed in Table 4. Compounds derived from Zr-DMBD *via* post-synthetic methods have extensive use spanning multiple domains. The applications are thoroughly discussed in the dedicated section on applications.

Yee *et al.* synthesized CAU-1 topological H_2DMBD (L_1)-based MOF by reacting with $AlCl_3{\cdot}6H_2O$, and this shows a surface area of 750 $m^2\ g^{-1}$ (Table 3, entry no. 2).[37] Munn *et al.* reported the isoreticular analogues of well-known MOF MIL-53 (Al) with the same ligand L_1 by changing the aluminium salt in 2016 (Table 3, entry no. 3).[108] The single-step synthesis of the MIL-53(Al)-SH was done by the solvothermal reaction between $Al(ClO_4)_3{\cdot}9H_2O$ and H_2DMBD in DMF solvent and used for iodine adsorption.

The conducting property of a H_2DMBD (L_1) containing MOF was reported by Dincă and co-workers in 2013 (Table 3, entry no. 4).[109] A nitrogen atmosphere reaction between $MnCl_2$ and L_1 (here denoted as H_4DSBDC instead of the generally used H_2DMBD) in DMF and methanol solvent leads to a conducting MOF $[Mn_2(DSBDC)(DMF)_2]{\cdot}0.2DMF$ containing a 1D $(-M-S-)_\infty$ chain. The solvent-free Mn_2(DSBDC) has charge mobility, similar to organic semiconductors. This was one of the significant reports in the category of conductive MOFs, which provide a roadmap for S-based ligands. The gas storage property of Mn_2(DSBDC) was studied by Runčevski *et al.*,[110] An extension work on the conductive Mn_2(DSBDC) was published after two years, in 2015, by Dincă and co-workers, where a

Table 3 Thiol-based MOFs with common structural motifs

Entry no.	Acronym name	Molecular formula	Ligand	Synthetic methodology	BET surface area ($m^2 g^{-1}$)	Structural motifs and dimensionality	Application	Ref.
1	Zr-DMBD	$Zr_6O_4(OH)_4 \cdot (DMBD)_6$	2,5-Dimercapto-1,4-benzenedicarboxylic acid (H_4DSBDC) or (H_2DMDB) (L_1)	Solvothermal	513	UiO-66 3D	Uptake of Hg(II), superprotonic conductivity, heterogeneous catalysis, photocatalysis	37 and 97–106
2	Al-DMBD	$[Al_4(OH)_2(OMe)_4(C_8H_4O_4S_2)_3] \cdot 8H_2O$		Solvothermal	750	CAU-1 3D	—	37
3	MIL-53(Al)-SH	$Al(C_8H_4O_4S_2)(OH) \cdot [H_2O]$		Solvothermal	324	MIL-53 3D	Iodine sequestration	108
4	Mn_2(DSBDC)	$Mn_2(DSBDC)(DMF)_2$		Solvothermal	232	MOF-74 3D	Conductive property and gas adsorption	109 and 110
5	Fe $_2$(DSBDC)	$Fe_2(DSBDC)(DMF)_2$		Solvothermal	54	MOF-74 3D	Conductivity	63
6	UiO-66-DCBDT	$Zr_6O_4(OH)_4(DCBDT)_{4.35}(H_2O)_{14}(CH_3COO)_{3.3}$	2,3-Dimercaptoterephthalic acid (L_3)	Hydrothermal	600	UiO-66 3D	Photocatalytic hydrogen evolution reaction	112
7	ZrDMTD	$Zr_6O_4(OH)_2(L_7)_6(DMF)_7(H_2O)_{18}$	2′,5′-Dimercapto-[1,1′:4′,1″-terphenyl]-4,4″-dicarboxylic acid (H_2DMTD) (L_7)	Solvothermal	136	UiO-68 3D	Catalytic activity in the Suzuki–Miyaura reaction	67
8	ZrDMBPD	$Zr_6O_4(OH)_4(DMBPD)_6(C_3H_7NO)(H_2O)_{35}$	3,3′-Dimercapto-[1,1′-biphenyl]-4,4′-dicarboxylic acid (H_2DMBPD) (L_6)	Solvothermal	792	UiO-67 3D	Catalytic activity in the Suzuki–Miyaura reaction	113
9	ZrOMTP	Zr_6O_4 $(OH)_4$ $(OMTP)_3$	4,4′,4″,4‴-(1,6-Dihydropyrene-1,3,6,8-tetrayl)tetrakis(2,6-dimercaptobenzoic acid) (H_4OMTP) (L_8)	Solvothermal	1443	NU-1100 3D	High efficiency in uptake of Hg(II)	114
10	Zr-L_9	$Zr_6O_4(OH)_4(L_9)_2(OH)_6(H_2O)_{27}(DMF)$	5′-(4-Carboxy-3,5-dimercaptophenyl)-3,3″,5,5″-tetramercapto-[1,1′:3′,1″-terphenyl]-4,4″-dicarboxylic acid (L_9)	Solvothermal	594	UMCM-309a 3D	Minimizing lead leaching in a perovskite solar cell	115
11	ZrTTA-6SH	$Zr_6O_4(OH)_4(HCOO)_{2.2}(OH)_5(C_{42}H_{24}N_3O_6S_6)_{1.6}(H_2O)_{25}$	4′,4‴,4⁗-(1,3,5-Triazine-2,4,6-triyl)tris(3,5-dimercapto-[1,1′-biphenyl]-4-carboxylic acid) (H_3TTA-6SH) (L_{10})	Solvothermal	265	UMCM-309a 3D	Photocatalytic hydrogen production	116
12	ZrTST	$Zr_6O_4(OH)_4(C_8H_4O_4S_4)_{3.8}(CH_3COO)_{4.4}(H_2O)$	2,3,5,6-Tetramercaptoterephthalic acid (H_2TST) (L_4)	Solvothermal	655	UiO-66 3D	Mercury removal and superprotonic conduction	117
13	Zr-MSA	$Zr_6O_4(OH)_4(MSA)_{5.61}FA_{0.78}$	2-Mercaptosuccinic acid (MSA) (L_{11})	Hydrothermal	513	UiO-66-FUM or MOF-801 3D	Cr and Hg removal	118 and 119
14	Zr-DMSA	-	2,3-Dimercaptosuccinic acid (DMSA) (L_{12})	Hydrothermal	275	UiO-66-FUM or MOF-801 3D	Hg removal	118

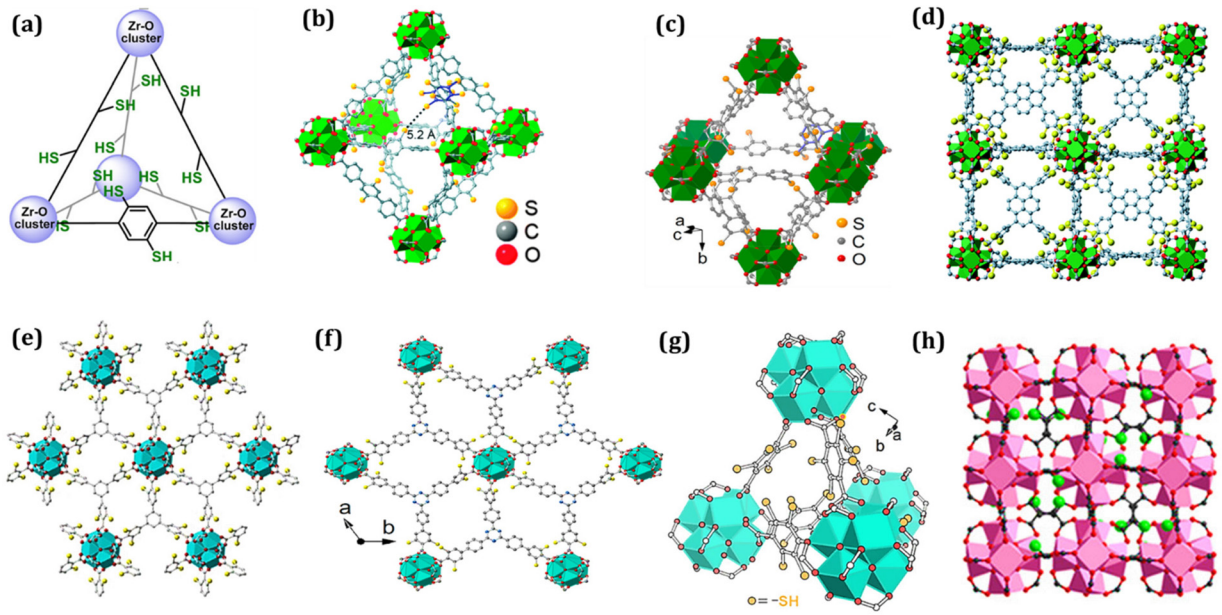

Fig. 7 Structure of thiol MOFs (a) Zr-DMBD,[37] (b) ZrDMTD,[67] (c) UiO-67-$(SH)_2$,[113] (d) ZrOMTP where O, C, S atoms and Zr polyhedra are designated as red, grey, yellow spheres and green polyhedra respectively,[114] (e) Zr-L_9,[115] (f) ZrTTA-6SH where Zr coordination polyhedra are displayed in green and N, S, O, and C atoms are displayed as blue, yellow, red, and grey beads, respectively,[116] (g) ZrTST,[117] (h) Zr-MSA, where the S atom is designated as a green sphere.[118] (Adapted with permission from the American Chemical Society, the Royal Society of Chemistry, Wiley-VCH and Elsevier Inc.)

Table 4 Post-synthetic modification of Zr-DMBD for various applications

Entry no.	Thiol-based MOF	Post synthetic modifications	Applications	Ref.
1	Zr-DMBD or UiO-66$(SH)_2$ or $Zr_6O_4(OH)_4$·$(DMBD)_6$	UiO-66$(SO_3H)_2$	High superprotonic conductivity	97
2		Zr-DMBD-Hg to Zr-$BDSO_3$-Hg	Acetylene hydration	98
3		Zr-DMBD-I_2	Catalyst for the iodo-cyclization reactions	99
4		UiO-66-$(SO_3H)_2$ and UiO-66-$(SCH_3)_2$	Photocatalytic property	100
5		Zr-DMBD-Co(II)	Visible-light-driven CO_2-to-CO conversion	101
6		Zr-DMBD-Hg	Vinylation transfer catalyst	102
7		Ag@Zr-DMBD	CO_2 fixation	103
8		UiO-66-$(SH)_2$@Pd	Quantitation of oligosaccharide	104
9		UiO-66-$(SH)_2$@PdmPtn	Colorimetric sensing of D-glucose and chlorophenol isomers	105
10		Au@UiO-66-$(SH)_2$	4-Nitrophenol hydrogenation reaction	106
11		Ag@Zr-DMBD	Reversible Li plating/stripping	107

million-fold enhancement of conductivity was achieved for Fe_2(DSBDC) by replacing the metal ion from Mn to Fe (Table 3, entry no. 5).[63] The reason proposed for the enhancement of the conductivity is the loose bonding of Fe^{2+} β-spin electrons. Both the $(–M–S–)_\infty$ chain-containing structures are closely related to MOF-74.[111]

Zhong *et al.* recently reported UiO-66-DCBDT (Table 3, entry no. 6) synthesized from thiol-based ligand L_3 with UiO-66 topology.[112] The presence of the thiol group in the 2,3 position of the ligand allows the incorporation of a transition metal by chelation (M = Fe, Ni or Cu) to synthesize UiO-66-DCBDT-M photocatalyst. Gui *et al.* reported ZrDMTD (Fig. 7b) from the extended thiol linker L_7, where the thiol groups are well separated with UiO-68 topology and 12-connected $Zr_6O_4(OH)_4$ clusters nodes connected with the DMTD linker containing a free-standing thiol group (Table 3, entry no. 7).[67] L_6 (H_2DMBPD)-containing zirconium MOF, namely Zr-DMBPD or UiO-67-$(SH)_2$, fills the synthetic gap between ZrDMBD and ZrDMTD (Table 3, entry no. 8).[113] Zr-DMBPD features the topology of UiO-67 (fcu topology) where $Zr_6O_4(OH)_4$ clusters are bridged by the linear H_2DMBPD linkers to generate UiO-67-$(SH)_2$ (Fig. 7c).

The thiol-containing Zr-OMTP (Table 3, entry no. 9) synthesized with ligand L_8 (H_4OMTP) was reported by Li *et al.*[114] The eight thiol group-containing ligand (H_4OMTP) solvothermally reacted with $ZrCl_4$ in the presence of benzoic acid as a modulator, and dithiol as a stabilizer, to form a polycrystalline framework of Zr-OMTP (Fig. 7d). Zr-OMTP is isoreticular

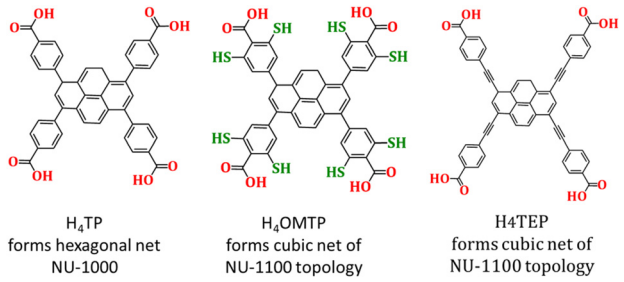

Fig. 8 Structural information of Zr-MOFs with three different tetracarboxylic acid linkers.

with NU-1100 (where the organic linker is 4-[2-[3,6,8-tris[2-(4-carboxyphenyl)ethynyl]-pyren-1-yl]ethynyl]-benzoic acid H_4TEP) (Fig. 8) which is a contrast to the expected NU-1000 (where the organic linker is unsubstituted 1,3,6,8-tetrakis(*p*-benzoic acid)pyrene (H_4TP)).[114] In 2020, Wu *et al.* reported a thiol functional 2D-MOF (3,6-connected) which was used as an electron extraction layer at the interface of a perovskite and cathode interface. Thiol-containing ligand L_9 (H_3L_9) is used to synthesize Zr-MOF (Table 3, entry no. 10),[115] The structure reveals that electronically hard Zr^{4+} metal centres bond with the electronically hard carboxylic acid group and leave thiol groups as free-standing groups, which offer benefits in perovskite solar cells (PVCs) (Fig. 7e). The structure also matches with MOF UMCM-309a derived from the tritopic linker H_3BTB (1,3,5-(4-carboxylphenyl)benzene).[120] The Zr MOF ZrTTA-6SH (Table 3, entry no. 11) reported with ligand L_{10} reveals that the ZrTTA-6SH crystallizes into a kgd net and is isoreticular to the known MOF UMCM-309a (Fig. 7f). The porphyrin-grafted material of the MOF shows high efficiency in the photocatalytic hydrogen evolution reaction.[116] Recently, He *et al.* reported a new dense thiol-based ligand (L_4) (H_2TST) and synthesized Zr-MOF (ZrTST) with same topology of UiO-66 as Zr-DMBD (Table 3, entry no. 12).[117] Zr-TST (Fig. 7g) shows excellent ability to remove mercury because of the enhancement of the free-standing thiol groups. Its oxidized form (where thiol groups are oxidized to $-SO_3H$) by m-CPBA (*meta*-chloroperoxybenzoic acid) shows the highest proton conductivity among the other sulfonate-equipped MOF materials. There are minimal reports available on thiol MOFs with aliphatic ligands. Yang *et al.* reported thiol MOF Zr-MSA (Fig. 7h and g) and Zr-DMSA using the aliphatic ligands mercaptosuccinic acid L_{11} (MSA) and dimercaptosuccinic acid L_{12} (DMSA) respectively (Table 3, entry no. 13 and 14).[118,119] The synthesis procedure is sustainable, unlike other thiol-based MOFs, where $ZrCl_4$ reacts with MSA and DMSA in water in the presence of a formic acid modulator. The structural analysis reveals that Zr-MSA and Zr-DMSA MOFs are iso-structural with the UiO-66-FUM with fcu topology, also called MOF-801.[121]

3.1.2.2 Thioether-based MOFs with common structural motifs. Like thiol-based MOFs, the concept of the HSAB principle is also applicable in thioether-based MOFs. When thioether-based ligands form MOFs with electronically hard metal ions, the thioether group of the ligand remains a free-standing group and generates structures with some well-known topology. Thioether-based MOFs with isoreticular MOF structures are listed in Table 5. Zhou *et al.* have reported Zn-TMBD (Table 5, entry no. 1) constructed with the thioether ligand L_{13} (TMBD); the thioether group remained as a free-standing group and forms an isoreticular MOF-5 structure (Fig. 8a).[84] He *et al.* reported a thioether-based MOF SESMOF-5 (Table 5, entry no. 2) in 2011 with the ligand L_{14}.[122] The structural study reveals that the compound is crystallized in the $Fm\bar{3}m$ space group with the formula $Zn_4O(L_{14})_3(DMF)_4(H_2O)_4$ and α-Po topology (*i.e.*, a simple cubic net) which is isoreticular with the MOF-5 structure, with a free-standing ($-SCH_2CH_2SCH_3$) group (Fig. 9b). Again in 2012, He *et al.*, reported a comparative study between two closely related Pb MOFs PbL_{14} and PbL_{15} synthesized from the ligands L_{14} and L_{15} (Table 5, entry no. 3 and 4).[123] The structure of PbL_{14}, where Pb(II) bonded with the carboxylic group of the ligand and only the S atom which is right next to the carboxylic group and the other S atom (that of $-SCH_3$) remains as a free-standing group, is similar to MOF-70 (PbBDC; BDC: 1,4-benzenedicarboxylate) (Fig. 9c). The PbL_{15} structure is similar to PbL_{14}, the only difference being that both the S and O atoms of the side chain are bonded with a common Pb ion (Fig. 9d). The structural difference leads to different properties; *e.g.*, the photoluminescence of PbL_{14} is yellowish-green, whereas PbL_{15} features bright white emission. Zirconium-based MOFs are generally 3D in structure, but Liu *et al.* in 2020 reported a unique 2D Zr-based MOF (USTS-7) with the ligand L_{14} (Table 5, entry no. 5).[64] The structure is not isoreticular to the UiO-66 system; instead, it has a 2D hexagonal lattice in a layer with UMCM-309 topology (Fig. 9e). USTS-7 is stable in a wide range of acidic and basic water solutions (pH 1 to 10). He *et al.* reported two thioether-based MOF, ASMOF-5 and ASUiO-66 (AS: allylthio) with L_{16} ligand, in 2013 and 2015, respectively (Table 5, entry no. 6 and 7).[124,125] ASMOF-5 crystalizes as an ($Fm\bar{3}m$) space group like MOF-5.[124] Zn_4O^{6-} nodes are present as a metal cluster in ASMOF-5 where the carboxylic group is bonded with the metal cluster, and the allyl-thioether groups are present as pendants groups (Fig. 9f). The corresponding Zr-MOF ASUiO-66 is isoreticular to UiO-66 where the allylthio group of the ligand remains as a free-standing group (Fig. 9g).[125]

Zr-TMBPD (Table 5, entry no. 8) containing TMBPD (L_{19}) ligand was reported by Wong *et al.*, and is isoreticular with UiO-67 (fcu topology) where $Zr_6O_4(OH)_4$ clusters act as an SBU and the ligand L_{19} as organic linker where the thioether groups remain as free-standing groups (Fig. 9h), which shows high stability in air, boiling water and a broad range of pH.[126] It also retains its structure after H_2O_2 oxidation. Burrows *et al.* synthesized two thioether-based Zn-MOFs (Table 5, entry no. 9 and 10) from a 4,4-biphenyldicarboxylate (BPDC) backbone containing the mono- and di-substitute thioether-based ligands L_{20} and L_{21}.[127] As the thioether ligand is not bonded with the metal, it forms structures similar to IRMOF-9. They have also synthesized corresponding sulfones by post-synthetic modifications (Fig. 9i). The unique thioether-based ligand L_{22}

Table 5 Thioether-based MOFs with common structural motifs

Entry no.	Acronym	Molecular formula	Ligand	Synthetic methodology	BET surface area (m^2 g^{-1})	Structural motif and dimensionality	Main application	Ref.
1	Zn-TMBD	$Zn_4O(H_2O)_3(TMBD)_3$	2,3,5,6-Tetrakis(methylthio) terephthalic acid (TMBD) (L_{13})	Solvothermal	—	MOF-5 3D		84
2	SESMOF-5	$Zn_4O(L_{14})_3(DMF)_4(H_2O)_4$	2,5-Bis(2(methylthio)ethylthio) terephthalic acid (L_{14})	Solvothermal	—	MOF-5 3D	Improve the stability, fluorescence, and metal uptake	122
3	PbL_{14}	$C_{14}H_{16}O_4PbS_4$	2,5-Bis(2-(methylthio)ethylthio) terephthalic acid (L_{14})	Solvothermal	—	MOF-70	Light emission	123
4	PbL_{15}	$C_{14}H_{16}O_6PbS_2$	2,5-Bis(((*S*)-2-hydroxypropyl)thio) terephthalic acid (L_{15})	Solvothermal	—	3D		
5	USTS-7	—	2,5-Bis(2-(methylthio)ethylthio) terephthalic acid (L_{14})	Solvothermal	108	UMCM-309 2D	Selective sensing of $Cr_2O_7^{2-}$	64
6	ASMOF-5	$Zn_4O{\cdot}(L_{16})_3{\cdot}(DEF)_2{\cdot}(H_2O)_2$	2,5-Bis(allylthio)terephthalic acid (L_{16})	Solvothermal	617	MOF-5 3D	Detection of palladium ions	124
7	ASUiO-66	$Zr_6O_4(OH)_2(L_{16})_5(HCOOH)$-$(DMF)_3(CH_3COOH)_4(H_2O)_{21}$		Solvothermal	566	UiO-66 3D	Extraction of palladium	125
8	Zr-TMBPD	$Zr_6O_4(OH)_4{\cdot}(C_{18}H_{16}O_4S_4)_6{\cdot}(DEF)_5{\cdot}(H_2O)_{37}$	3,3′,5,5′-Tetrakis(methylthio)-[1,1′-biphenyl]-4,4′-dicarboxylic acid (H_2TMBPD) (L_{19})	Solvothermal	1153	UiO-67 3D	High stability in wide pH range	126
9	—	$[Zn_4O(L_{20})_3(DMF)_2]{\cdot}4DMF$	3-((Methylthio)methyl)-[1,1′-biphenyl]-4,4′-dicarboxylic acid (L_{20})	Solvothermal	—	IRMOF-9 3D	Stable to oxidation	127
10	—	$[Zn_4O(L_{21})_3]{\cdot}5DMF$	3,3′-Bis((methylthio)methyl)-[1,1′-biphenyl]-4,4′-dicarboxylic acid (L_{21})	Solvothermal	—	IRMOF-9 3D	Stable to oxidation	127
11	Zr-L_{22}	$Zr_6O_4(OH)_4(L_{22})_6$	4,4′-(Buta-1,3-diyne-1,4-diyl)bis(3-(3-(methylthio)-2,2-bis((methylthio) methyl)propoxy)benzoic acid) (L_{22})	Solvothermal	—	UiO-68 3D	Hg adsorption	128
12	Zr-L_{23}	$Zr_6O_4(OH)_6(H_2O)_2$ $(L_{23})_5(DMF)_5(H_2O)_3$	2′,5′-Bis((3-(methylthio)-2,2-bis ((methylthio)methyl)propyl)thio)-[1,1′:4′,1″-terphenyl]-4,4″-dicarboxylic acid (L_{23})	Solvothermal	341	UiO-68 3D	Hg adsorption	129
13	Zr-L_{24}	$Zr_6O_4(OH)_8(H_2O)_4(L_{24})_4(H_2O)_9$	4,4′-(Buta-1,3-diyne-1,4-diyl)bis(3-(3-((4-methoxyphenyl)thio)-2,2-bis ((methylthio)methyl)propoxy) benzoic acid) (L_{24})	Solvothermal	189	UiO-68 3D		
14	Zr-L_{25}	$Zr_6O_4(OH)_8(H_2O)_4(L_{25})_2(H_2O)_7$	4,4′,4″,4‴-(Pyrene-1,3,6,8-tetrayltetrakis(ethyne-2,1-diyl)) tetrakis(3-(3-(methylthio)-2,2-bis ((methylthio)methyl)propoxy) benzoic acid) (L_{25})	Solvothermal	250	NU-1100 3D		

Table 5 *(Contd.)*

Entry no.	Acronym	Molecular formula	Ligand	Synthetic methodology	BET surface area (m^2 g^{-1})	Structural motif and dimensionality	Main application	Ref.
15	Zr-BPDC-3S5F	$Zr_6O_4(OH)_4(BPDC\text{-}3S5F)_{5.1}(HCOO)_{1.8}(H_2O)_2$	2,2′,3,3′,5,6′-Hexafluoro-5′,6-bis (methylthio)-[1,1′-biphenyl]-4,4′-dicarboxylic acid (H_2BPDC-3S5F) (L_{27})	Solvothermal	986	UiO-67, 3D	Proton conductivity	130
16	Zr-BPDC-4S4F	$Zr_6O_4(OH)_4(bpdc\text{-}4S4F)_4(HCOO)_4(H_2O)_3$	2,2′,5,5′-Tetrafluoro-3,3′,6,6′-tetrakis (methylthio)-[1,1′-biphenyl]-4,4′-dicarboxylic acid (H_2BPDC-4S4F) (L_{28})	Solvothermal	835			
17	Zr-BPDC-6S2F	$Zr_6O_4(OH)_4(BPDC\text{-}6S2F)_{3.4}(HCOO)_{5.2}$	2,5-Difluoro-2′,3,3′,5′,6,6′-hexakis (methylthio)-[1,1′-biphenyl]-4,4′-dicarboxylic acid (H_2 BPDC-6S2F) (L_{29})	Solvothermal	657			
18	Zr-BPDC-8MS	$Zr_6O_4(OH)_4$ $(BPDC\text{-}8MS)_{3.2}(HCOO)_{5.6}(CH_3OH)_{9.5}$	2,2′,3,3′,5,5′,6,6′-Octakis (methylthio)-[1,1′-biphenyl]-4,4′-dicarboxylic acid (H_2 BPDC-8MS) (L_{30})	Solvothermal	449			
19	ZrBPD-4F4TS	$Zr_6O_4(OH)_4(BPD4F4TS)_{3.8}(HCOO)_{4.4}(H_2O)_6$	2,2′,5,5′-Tetrafluoro-3,3′,6,6′-tetrakis (thiophen-2-ylthio)-[1,1′-biphenyl]-4,4′-dicarboxylic acid (L_{31})	Solvothermal	177	UiO-67 3D	Conductivity	131

containing a pentaerythrityl side chain and equipped with three-pronged thioether donors was synthesized and utilized for the synthesis of a new thioether-based MOF namely Zr-L_{22} by the solvothermal reaction between the ligand L_{22} and $ZrCl_4$ (Table 5, entry no. 11).[128] The crystal structure of Zr-L_{22} was not suitable for SCXRD analysis due to weak diffraction spots, so the initial analysis was done by NMR spectroscopy, which indicates the structural formula is $[Zr_6O_4(OH)_4(L_{22})_6]$ associated with guest molecules like benzoic acid, DEF, and water. The PXRD pattern also indicates towards a UiO prototype where the linear linkers bridge $Zr_6O_4(OH)_4$ clusters, but when the crystal Zr-L_{22} was loaded with $HgCl_2$ (Zr-L_{22}-$HgCl_2$), it can be easily solved (Fig. 9j) by SXRD due to the improvement of the diffraction spots (Fig. 10). The MOF Zr-L_{22} is efficient for mercury adsorption applications because regular thioether groups bind with mercury covalently, which complicates the adsorbent recycling process, but in this case, thioether binds with mercury by chelation, and extricating mercury is easier.

He *et al.* synthesized Zr MOFs by utilizing the ligands L_{22}, L_{23}, L_{24} and L_{25} (Table 5, entry no. 12–14).[129] Zr-L_{23} (Fig. 9k) is isoreticular with UiO-68 with free-standing thioether groups. Zr-L_{22} and Z-L_{24} (Fig. 9l) are isostructural. ^{128}Zr-L_{25} (Fig. 9m) is isoreticular with cubic NU-1100. The stability order of the different MOFs is Zr-L_{22} < Zr-L_{25} < Zr-L_{24} < Zr-L_{23}.

Xian *et al.* reported a series of stable MOFs by fluorine-containing thioether-based ligands with zirconium (Table 5, entry no. 15–18).[130] They have synthesized thioether-based linkers with precisely controlled thioether numbers and positions L_{27}–L_{30}. These MOFs are structural prototypes of the UiO-67 framework with high stability. The self-assembly synthesis of the MOF (ZrBPD-4F4TS) was done by the solvothermal reaction between $ZrCl_4$ and L_{31} (H_2BPD-4F4TS) in DMF solvent with the help of a trifluoroacetic acid modulator (Fig. 9n).[131] The MOF ZrBPD-4F4TS (Table 5, entry no. 19) crystallizes in the $F\bar{4}3m$ space group and features $Zr_6O_4(OH)_4(CO)_{12}$ clusters in a face-centered cubic (fcc) array, which are connected by the ligand BPD-4F4TS and generate fcu topology, and are isoreticular with UiO-67 (Fig. 9o). The reported MOF shows electronic conductivity of 1.1×10^{-5} S cm^{-1}, and a band-gap of 2.75 eV. The electronic conductivity increases about 200 times (2.2×10^{-5} S cm^{-1}) in the case of crystalline ZrBPD-4F4TS-Ox (band-gap 1.66 eV) synthesized from ZrBPD-4F4TS by oxidative treatment by $FeCl_3$ because it couples the thiophene units of the MOF to form a covalent conjugate bridge. The cross-linked solid ZrBPD-4F4TS-Ox also shows proton conductivity which can be broadly increased by acid (H_2SO_4) treatment (*e.g.*, from 5.0×10^{-7} to 1.6×10^{-3} S cm^{-1}).

3.2 Synthesis by indirect methods

3.2.1 Post-synthetic modifications. Post-synthetic modifications are a vital tool for synthesizing thiol and thioether-based MOFs, as only a limited number of associated ligands are available.[132] The key advantage of this technique is that the topology of the MOF remains unchanged. Robust MOFs containing free amine groups are widely used for introducing sulfur functionality *via* reactions with sulfurizing agents like

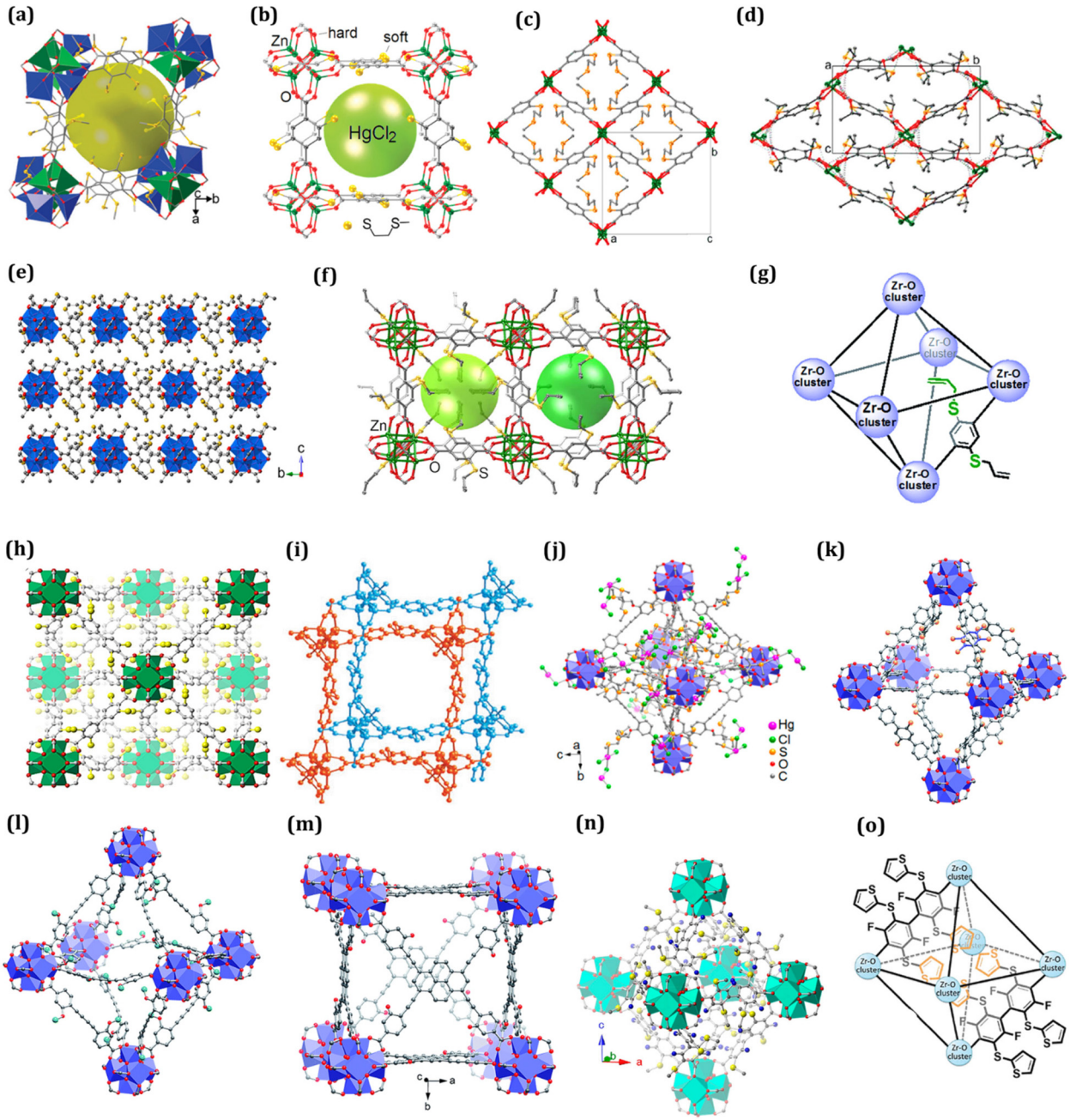

Fig. 9 (a) 3D coordinate structure of Zn-TMBD,[84] (b) crystal structure $Zn_4O(L_{14})_3(DMF)_4(H_2O)_4$ with a cavity,[122] (c) crystal structure of PbL_{14},[123] (d) crystal structure of PbL_{15},[123] (e) crystal structure of USTS-7 when seen along an axis; C, O, and S atoms are depicted as grey, red, and yellow spheres; Zr_6 clusters are shown in blue,[64] (f) two-face-sharing crystal structure of ASMOF-5,[124] (g) pictorial representation of the crystal structure of ASUiO-66,[125] (h) single-crystal structures of the Zr-TMBPD unit cell of the cubic framework where Zr-SBU – green, O – red, S – yellow, and C – grey,[126] (i) $[Zn_4O(L_{20})_3(DMF)_2]\cdot 4DMF$,[127] (j) structure of Zr-L_{22},[128] (k) Zr-L_{23},[129] (l) Zr-L_{24},[129] (m) Zr-L_{25},[129] (n) Zr-BPDC-4S4F framework where Zr coordination polyhedra are depicted as cyan and O, S, C, and F atoms are depicted as red, yellow, grey, and blue spheres,[130] (o) pictorial representation of the crystal structure of ZrBPD-4F4TS.[131] (Adapted with permission from the American Chemical Society, the Royal Society of Chemistry, Wiley-VCH and Elsevier Inc.)

thioglycolic acids (Fig. 11). Thiol-based MOFs synthesized by the PSM strategy are listed in Table 6. In 2015, Cheng *et al.* incorporated the thiol group in an MIL-53(Al) framework by reacting NH_2-MIL-53(Al) with thioglycolic acid (Table 6, entry no. 1).[133] Due to the free thiol group's presence, it can stabilise the Ag nanoparticle. In 2019 Li *et al.* used the same strategy to synthesize SH-MIL-68(In) from MIL-68(In)-NH_2 (Table 6, entry no. 2).[68] Deng *et al.* also reported a Pd nanoparticle encapsulated thiol-based MOF by installing the thiol group in UiO-66-NH_2 by the same strategy, which shows high catalytic

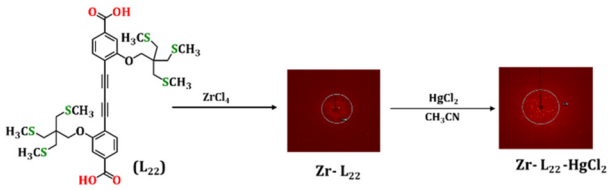

Fig. 10 Synthesis of an SC-XRD suitable crystal.[128] (Reproduced with permission from the American Chemical Society.)

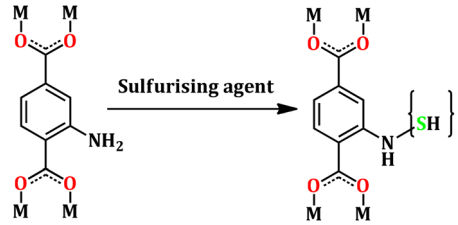

Fig. 11 General strategy for synthesizing thiol-based MOF from amine-based MOFs.

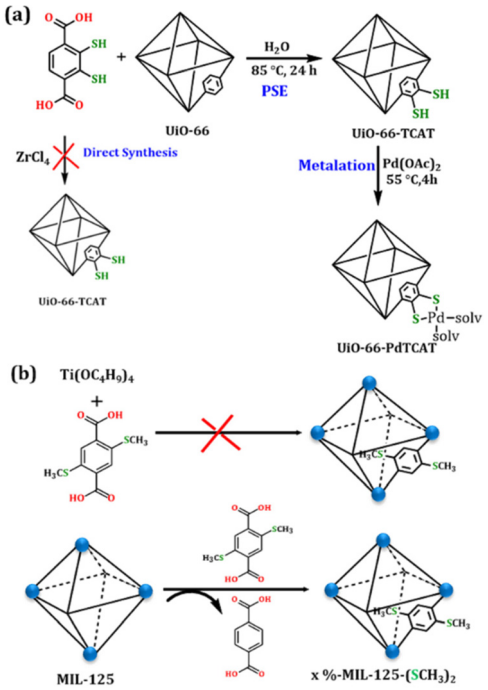

Fig. 12 (a) Synthesis of UiO-66-TCAT and UiO-66-PdTCAT,[136] (b) synthesis of MIL-125-$(SCH_3)_2$.[137] (Reproduced with permission from the American Chemical Society and Wiley-VCH.)

efficiency (Table 6, entry no. 3).[134] A Ag nanoparticle incorporated thiol MOF, which was synthesized by the post-synthetic modification of NH_2-MIL-101(Cr) reported by Liu *et al.*, shows good photocatalytic RhB dye degradation and CO_2 fixation capability (Table 6, entry no. 4).[135] A three sulfur atom-containing moiety 2,5-dimercapto-1,3,4-thiadiazole was introduced in the UiO-66-NH_2 framework by Fu *et al.*, where thiol reacts with the amine group of the pristine MOF to form UiO-66-DMDT *via* S–N bond formation (Table 6, entry no. 5).[66]

3.2.2 Post-synthetic exchange. Direct and PSM synthesis may fail to produce the desired thiol and thioether-based MOFs in various instances. Post-synthetic exchange (PSE) may be useful and viable to overcome this. This strategy is mainly utilized for making corresponding thiol and thioether-based MOFs of UiO-66. In 2015 Fei *et al.* reported the synthesis of UiO-66-TCAT where the direct synthesis route of the solvothermal reaction between 2,3-dimercaptoterephthalate acid (TCAT) and $ZrCl_4$ was unsuccessful.[136] In this method, the reaction between 2,3-dimercaptoterephthalate acid (TCAT) and UiO-66 leads to UiO-66-TCAT (Fig. 12a). The thiocatechol group of the MOF UiO-66-TCAT was utilized for metalation by soft metal palladium and UiO-66-PdTCAT, which act as a very efficient heterogeneous catalyst. In 2018 Han *et al.*, reported a photocatalyst as *x*%-MIL-125-$(SCH_3)_2$ (where x = 20 and 50%) using MIL-125 reacts with L_{18} H_2BDC-$(SCH_3)_2$ (Fig. 12b).[137] Recently, Muhamed *et al.* reported NU-1000-SH where 2-MBA (2-mercapto-benzoic acid) was introduced in the MOF structure by a solvent-assisted ligand incorporation (SALI) procedure (Fig. 12c).[138] Finally, Ag and Au nanoparticles were immobilized in NU-1000-SH to form Ag@ NU-1000-SH and Au@ NU-1000-SH, both of which are efficient catalysts for the hydrogen evolution reaction.[138,139]

3.2.3 Synthesis by the mixed linker strategy. Recently, Mandal and co-workers synthesized a defective thiol-based UiO-66-SH-10 by the reaction between $ZrCl_4$, terephthalic acid and 2-MBA (2-mercapto-benzoic acid) as a modulator (Fig. 13).[140] The modulator 2-MBA slows down the reaction process and creates a defect in the structure, installing the thiol group in the MOFs. After synthesizing, Pd nanoparticles

Table 6 MOFs synthesized by the PSM strategy

Entry no.	MOFs	Organic ligand	Sulfurizing agent	Surface area	Applications	Ref.
1	HS-MIL-53(Al)	H_2BDC-NH_2	Thioglycolic acid	2610	Stabilization of Ag nanoparticles	133
2	SH-MIL-68(In)		Thioglycolic acid	287	Hg adsorption	68
3	UiO–CH_2SH/ UiO–PHSH		Mercaptoacetic acid, 2-mercaptobenzoic acid	—	Efficient catalytic hydrogenolysis of biomass-derived aromatic aldehydes	134
4	NH_2-MIL-101 (Cr)-s		Thiomercaptanoic acid	—	Photocatalytic degradation of RhB dye and CO_2 fixation	135
5	UiO-66-DMDT		2,5-Dimercapto-1,3,4-thiadiazole	651	Hg removal from water	66

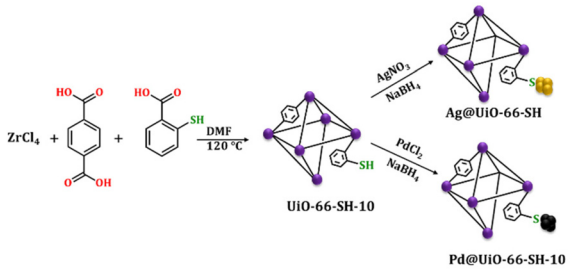

Fig. 13 Synthesis of thiol-based MOFs by a mixed linker strategy.[140] (Adapted by taking permission from the Royal Society of Chemistry.)

were incorporated, which can photocatalytically reduce Cr(IV). In the same MOF UiO-66-SH-10, Ag nanoparticles are incorporated, which act as an efficient catalyst for A^3 coupling reactions and electrocatalytic CO_2 reduction.[141,142] Moll *et al.* introduce thiol functionality in the Zr cluster by adding thioglycolic acid while synthesizing UiO-66, which eventually synthesizes UiO-66-Mac, showing improved Ag(I) uptake capacity from aqueous solutions.[143]

3.2.4 Composite materials. Numerous MOFs have been synthesized over the last four decades, but only a small number have found commercial success due to their drawbacks in actual working environments. The potential use of MOFs in composite materials is encouraging because the strength of the MOFs increases dramatically in many composites.[144] Preparing the composite material from MOFs is essential for using thiol and thioether-based MOFs on an industrial scale.

Some of the stable thiol MOFs like Zr-DMBD are used widely for the synthesis of well-constructed composite materials. In 2020 Yang *et al.* reported a 3D macroporous carbon/Zr-2,5-dimercaptoterephthalate nano-composite (Table 7, entry no. 1) that shows excellent efficiency in removing and detecting Hg(II).[145] Nano-composite Zr-DMBD MOFs/3D-KSC were synthesized solvothermally by the *in situ* inert atmosphere reaction between $ZrCl_4$, H_2DMBD, and 3D-KSC in DMF solvent (Fig. 14a). Microscopic studies (SEM) reveal that

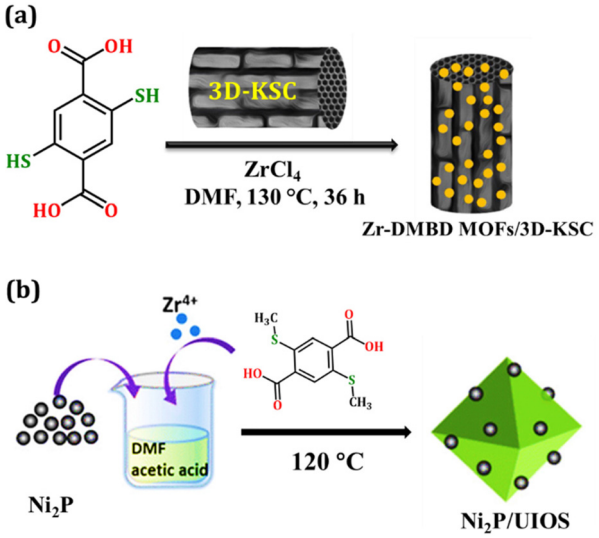

Fig. 14 (a) Schematic diagram of the synthesis of Zr-DMBD MOFs/3D-KSC and Hg(II) detection,[145] (b) Synthesis of Ni_2P/UIOS.[151] (Adapted with permission from Elsevier Inc and the Royal Society of Chemistry.)

Zr-DMBD MOFs are dispersed uniformly on 3D-KSC in the composite, which leads to uniformly grown free thiol groups on the surface of the 3D-KSC. In recent years, MOFs have become a promising photocatalyst for the photodegradation of organic pollutants.[86] MOFs combined with semiconductor nanoparticles have been investigated for photocatalysis, such as MIL-88, which interacts with a variety of semiconducting materials and exhibits high photocatalytic activity.[146] The stable thiol-based MOF Zr-DMBD or UiO-66-$(SH)_2$ shows photocatalytic activity for the degradation of RhB under visible light because of its effective electron transfer and simultaneously $ZnIn_2S_4$, a stable semiconductor, acts as an excellent photocatalyst for hydrogen production. In 2019 Chen *et al.* reported a series of composite materials of UiO-66-$(SH)_2$ and $ZnIn_2S_4$ named ZIS/US, which showed high photocatalytic activities for the degradation of RhB (Table 7, entry no. 2).[147] In 2020, Boix *et al.* incorporated CeO_2 and Fe_3O_4 nanoparticles in the UiO-66$(SH)_2$ to form the nanocomposite CeO_2/

Table 7 Composite of thiol-based MOFs

Entry no.	MOF	Matrix	Composite	Applications	Ref.
1	Zr-DMBD	3D-KSC	Zr-DMBD MOFs/3D-KSC	Removal and detection of Hg(II)	145
2	Zr-DMBD	$ZnIn_2S_4$	$ZnIn_2S_4$/UiO-66-$(SH)_2$	Visible-light photocatalyst for RhB degradation	147
3	Zr-DMBD	Cerium-oxide nanoparticles	CeO_2/Fe_3O_4@UiO-66-$(SH)_2$	Heavy metal adsorption	148
4	Zr-DMBD	CdS/ZnS quantum dots to the Cu-decorated Zr-DMBD	UiOS-Cu-CdS/ZnS	Photocatalytic hydrogen evolution	149
5	Zr-DMBD	Carbon cloth	CC@ UiO-66$(SH)_2$	Integrated interlayer–current collector for Li–S batteries	150
6	UiO-66-$(SCH_3)_2$(UIOS)	Ni_2P NP	Ni_2P/UIOS	Photocatalytic hydrogen evolution	151

Fe_3O_4@UiO-66-$(SH)_2$, which can simultaneously remove heavy metals from river water samples (Table 7, entry no. 3).[148] Mao *et al.* synthesized UiOS-Cu by fabricating CdS/ZnS quantum dots in thiol-functionalized UiO-66. UiOS-Cu acts as an efficient photocatalyst for hydrogen evolution reactions (Table 7, entry no. 4).[149]

Recently Liu *et al.* reported a composite material CC@UiO-66$(SH)_2$ where UiO-66$(SH)_2$ nanoparticles grow *in situ* on the carbon cloths (CC), which act as an interlayer current collector for Li–S batteries (Table 7, entry no. 5).[150] A Ni_2P nanoparticle-incorporated thioether-based MOF composite was synthesized by Li *et al.* by an *in situ* impregnation technique (Table 7, entry no. 6), which was utilized for photocatalytic hydrogen evolution reactions (Fig. 14b).[151]

4. MOFs containing only thiol-thioether-based ligands

Metal–thiolate bonding is extensively studied in inorganic chemistry, but for synthesizing thiol and thioether-based MOFs, much attention was given towards thiol and thioether-based MOFs with carboxylic acid linkers.[152–154] However, in recent years, many MOFs with only thiol and thioether-containing ligands have been synthesised, showing the potential towards newer avenues.[71]

4.1 MOFs containing only thiol-based ligands

There has been significant interest in two-dimensional (2D) materials such as graphene,[155] covalent organic frameworks (COFs),[156] metal–organic layers (MOLs),[157] and metal–organic nanosheets (MONs)[158] *etc.* due to their notable conductivity and distinctive electrical properties.[159,160]

Linkers containing bis(dithiolato), bis(diimino), and bis(catecholato) have been used extensively to synthesize 2D conductive MOFs as they have p-conjugated systems with flat molecular structures, and the p-conjugated system spreads over the nanosheets when metal complexes are formed.[161,162] Thiol-containing ligands like benzenehexathiol (BHT/HTB), triphenylenehexathiol (THT/HTT), 1,2,3,4,5,6,7,8,9,10,11,12-perthiolated coronene (PTC), and benzene-1,2-dithiol (BDT) (Fig. 15) are ideal for synthesizing conductive MOFs because the p orbital of a dithiolate ligand and the d orbital of a metal centre synergize to create quasi-aromaticity, enabling electron delocalization across the five-membered metalladithiolene ring.[163–165] In accordance with this principle, numbers of thiol-based MOFs have been synthesized and utilized mostly for conductive applications.

Generally, this type of MOF is synthesized by an interface-assisted synthesis methodology. Benzenehexathiolate (BHT/HTB) is an important ligand in the category of thiol-based ligands, and a wide range of MOFs have been synthesized over the years. Generally, BHT-based MOFs show two types of structure, $M_3(BHT)_2$ and M_3BHT (Fig. 16), depending on the metal ions. Usually, when cobalt (Co), palladium (Pd) or platinum (Pt) ions are used as the metal centre, the resulting MOFs

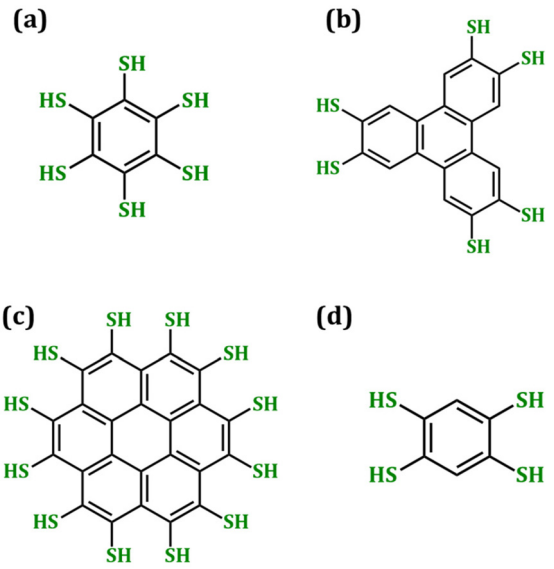

Fig. 15 Linker for thiol-based MOFs: (a) benzenehexathiol (BHT/HTB), (b) triphenylenehexathiol (THT/HTT), (c) 1,2,3,4,5,6,7,8,9,10,11,12-perthiolated coronene (PTC), (d) benzene-1,2,4,5-tetrathiol (BTT).

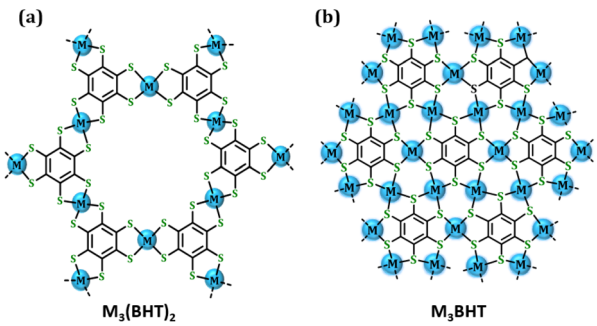

Fig. 16 Structure of BHT/HTB-based MOFs.

exhibit a porous $M_3(BHT)_2$ structure. In contrast, most other metal ions lead to the formation of the densely-packed M_3BHT structure. Interestingly, Nickel (Ni) shows both types of structure.

The utilization of BHT/HTB to synthesize MOFs was initially started by Kambe *et al.*, where the pi-conjugated 2D semiconducting material $Ni_3(BHT)_2$ was synthesized by a liquid–liquid interfacial reaction between BHT in the organic phase and nickel(II) acetate in the aqueous phase (Table 8, entry no. 1).[71,162] Recently, Banda *et al.* synthesized nonporous Ni_3BHT, which behaves as an pseudocapacitor.[166] In 2015 Pal *et al.*, synthesized $Pd_3(BHT)_2$ by an interface-assisted synthesis method in the presence of oxidizing buffer $K_3[Fe(CN)_6]$ which prevents the formation of Pd^0 nanoparticles (Table 8, entry no. 2).[167] Interface-assisted synthesis was also utilized by Huang *et al.* to synthesize a 2D coordination polymer $Cu_3(BHT)$ with exceptionally high conductivity (Table 8, entry no. 3).[168] Structurally, the ligand BHT binds with six Cu^{II}, which enhances the framework density and lowers the porosity. Later

Table 8 MOF synthesized from thiol-based linkers

Entry no.	Thiol ligand	MOFs	Synthetic method	Ref.
1	Benzenehexathiol (BHT/HTB)	NiBHT	Interface-assisted synthesis	71, 162 and 166
2		PdDT	Interface-assisted synthesis	167
3		Cu-BHT	Interface-assisted synthesis	168–171
4		Cu_3(BHSe)	Homogeneous reaction	172
5		Ag-BHT	Interface-assisted synthesis	163
6		Ag_3BHT_2	Interface-assisted synthesis	173
7		Au_3BHT_2	Interface-assisted synthesis	173
8		CoBHT	Interface-assisted synthesis	174
9		FeBHT	Interface-assisted synthesis	73
10	Triphenylenehexathiol (THT/HTT)	$Pt_3(HTT)_2$	Interface-assisted synthesis	72
11		$Fe_3(THT)_2(NH_4)_3$	Interface-assisted synthesis	175
12		$Co_3(THT)_2$	Interface-assisted synthesis	176
13		Solvent-free $Fe_3(THT)_2$ and $Co_3(THT)_2$	Interface-assisted synthesis	177
14		THTA-M (M = Co and Ni)	Interface-assisted synthesis	178
15		THTNi	Interface-assisted synthesis	179
16		CoTHT	Interface-assisted synthesis	174
17	1,2,3,4,5,6,7,8,9,10,11,12-perthiolated	Fe-PTC	Solvothermal synthesis	165
18	coronene (PTC)	Co-PTC	One-pot reflux	180
19		Ni-PTC	Homogeneous reaction	181
20	Benzene-1,2,4,5-tetrathiol (BTT)	FeBTT	Interface-assisted synthesis	182
		CoBTT	Interface-assisted synthesis	183
		NiBTT	Interface-assisted synthesis	164
		ZnBTT	Interface-assisted synthesis	182

Huang *et al.* reported a significantly crystalline Cu-BHT with a perfect kagome structure, which again enhanced the conductivity of the sample.[170] The selenite analogoue of BHT, benzenehexaselenol (H_6BHS), was utilized to synthesize the 2D π–d conjugated conductive coordination polymer Cu_3(BHSe) by a homogeneous reaction between cupric ions and H_6BHS (Table 8, entry no. 4).[172] Huang *et al.* reported highly crystalline films of a silver-based coordination polymer $[Ag_5(C_6S_6)]_n$ (Ag-BHT), which is structurally different from $Ni_3(BHT)_2$ as well as Cu_3(BHT) (Table 8, entry no. 5).[163] The structure of Ag-BHT is formed by many Ag–Ag and Ag–S–Ag chains which are responsible for their charge transport behaviour. Chen *et al.* synthesized Ag_3BHT_2 and Au_3BHT_2 by a liquid–liquid interfacial reaction; these are structurally related to Cu_3(BHT) (Table 8, entry no. 6 and 7).[173] A gas–liquid interfacial reaction was utilized by Clough *et al.* for synthesizing the 2D electrocatalyst Co-BHT which adopts a $M_3(BHT)_2$ structure (Table 8, entry no. 8).[174] Downes *et al.* synthesized FeBHT by a similar interfacial assisted method, which is also an efficient electrocatalyst for the HER (Table 8, entry no. 9).[73]

Cui *et al.* synthesized conducting $Pt_3(HTT)_2$ by the reaction between 2,3,6,7,10,11-hexakis(butyrylthio)triphenylene (HBuTT) and $Pt(CH_3CN)_2Cl_2$ with permanent porosity (Table 8, entry no. 10).[72] The synthesized material is anionic and forms an almost neutral framework upon oxidation. The compound is not highly crystalline due to the strong covalent interaction between the thiol and platinum. However, based on the unit cell calculation, a structural model was presented in which square-planar Pt^{II} ions connect the ligands. Dong *et al.* synthesized conductive $Fe_3(THT)_2(NH_4)_3$ by liquid–liquid interfacial synthesis where the structure is composed of an iron-bis (dithiolen) linkage and NH_4^+ counter-ions, which gives the semiconducting property to the material (Table 8, entry no. 11).[175] The material is not highly crystalline in nature; however, from PXRD and HRTEM, it was found to have a layered honeycomb structure similar to $Pt_3(THT)_2$. Clough *et al.* synthesized a conductive 2D MOF $Co_3(THT)_2$ exhibiting a structure similar to $Pt_3(THT)_2$ with better crystallinity (Table 8, entry no. 12).[176] The significantly improved conductive property of guest-free $Co_3(THT)_2$ and $Fe_3(THT)_2$ was studied in 2019 (Table 8, entry no. 13).[177] Dong *et al.* synthesized 2D molecular metal dithiolene–diamine complexes (THTA-M, M = Co and Ni) which act as an electrocatalyst (Table 8, entry no. 14).[178] A gas–liquid interfacial reaction was utilized by Dong *et al.* to synthesize an electrocatalyst THTNi, which has a thickness of 0.7–0.9 nm (Table 8, entry no. 15).[179] CoTHT was synthesized by Clough *et al.* and also acts as an electrocatalyst for the HER reaction (Table 8, entry no. 16).[174] Dong *et al.* have reported a very interesting result by synthesizing a 2D semiconducting Fe MOF, Fe-PTC from a coronene-based thiol ligand (PTC = perthiolated coronene) (Table 8, entry no. 17).[165] In contrast to the usual catechol-like mode found in $Pt_3(THT)_2$, the thiols in the nanoporous Fe-PTC exhibit coordination modes more akin to acetylacetonate. Later Chen *et al.*, synthesized 2D electrocatalyst Co-PTC[180] for the HER and Ni-PTC for thermoelectric conversion (Table 8, entry no. 18 and 19).[181] Downes *et al.* synthesized three 1D metal dithiolene (M = Ni, Fe, Zn) coordination polymers with benzene-1,2,4,5-tetrathiolate (BTT) by a liquid–liquid interfacial synthesis method (Table 8, entry no. 20).[182] The cobalt analogous CoBTT was synthesized by Downes *et al.* by gas–liquid interfacial synthetic methodology.[183] Fe and Zn-dithiolene (FeBTT and ZnBTT) are inactive for the HER reaction, and between Co and Ni-dithiolene, NiBTT shows better HER efficiency.[164]

4.2 Thioether-containing MOFs

Xiao *et al.* utilized the SALI strategy to synthesize MOF-A, which was unsuccessful, by the direct reaction between the thioether-based ligand 1,4-dibromo-2,3,5,6-tetrakis(4-carboxyphenyl)benzene carboxylates (TCPBBr), 4-((pyridin-4-ylthio) methyl)pyridine (Ls) and $Zn(NO_3)_2{\cdot}6H_2O$.[184] MOF-A was utilized for heavy metal uptake.

5. MOFs containing thiol-thioether-based azolate ligands

There are only a handful of reports on thiol-thioether-based azolate linkers containing MOFs. Pyrazolate-based MOFs are well-known for their stability in comparison with carboxylate-based MOFs.[185] Introduction of the sulfur functionality is a challenging task, and their stability remains a challenge.[186] Yang *et al.* introduced thiol functionality in a free amine-containing pyrazolate MOF by reacting with thioglycolic acid (PSM strategy).[74] The Ag(I)anchored thiol MOF was utilized as a catalyst for a CO_2 fixation reaction. Yang *et al.* synthesized a flexible MOF PCN-41, by using a thioether-based triatopic linker (1,3,5-tris(4-pyridylsulfanylmethyl)-2,4,6-trimethylbenzene) and star-like $\{Cu_4I_4\}$ cluster.[75] This triazine-based material can act as a crystalline sponge for the structural characterization of liquid organic molecules like dimethylformamide (DMF), methyl cyanide (MeCN), *N*-methyl-2-pyrrolidone (NMP), dimethyl sulfoxide (DMSO) and benzaldehyde (CH_3CHO). Gai *et al.* introduced a novel strategy to form a ZIF-8-type (CPM-8S) net with disulfide bonds between the triazolate linkers by reacting $ZnCl_4$ and a triazole-based thiol linker (1,2,4-triazole-3-thiol).[76] In the structure of CPM-8S, Zn(II) is tetrahedrally coordinated by four nitrogen atoms of three DS-TRZ (where DS-TRZ is bis(1,2,4-triazole-3-yl)-disulfide, which generates *in situ*) ligands by both chelating and bridging modes, which create a sodalite type structure ($4^2{\cdot}6^4$) and can be utilized for ethane/ethylene separation. Hu *et al.*, synthesized a cruciform linker with pyrazolate and thioether functional groups followed by the corresponding Ni-MOF.[187] The $[Ni_8(OH)_4(H_2O)_2]$ cluster containing MOF shows fcu topology and can act as an efficient electrocatalyst.

6. Applications

Thiol and thioether-based MOFs are extensively employed in a wide range of applications due to their distinctive characteristics such as tunability, stability, porosity, and electronically diverse functional groups. These applications include catalysis, sensing, heavy metal adsorption, conductivity, photocatalysis, and gas storage. The following sections will provide discussions on each of the significant applications.

6.1. Heterogeneous catalysis

A catalytically active MOF could be a heterogeneous catalyst with reaction medium stability and reusability.[11] There are distinct advantages of using MOF as a heterogeneous catalyst, such as MOF with intrinsic catalytic activity, where the catalytic activity of MOFs originates from open metal sites (coordinatively unsaturated sites), defects, or catalytically active organic linkers.[188] In the case of thiol and thioether MOFs, the catalytic activity is due to the introduction of active metal centres like Pd, Au, Ag *etc*.[189] The reactive nature of the thiol or thioether group towards soft metal ions plays a vital role in introducing catalytically active metals in thiol and thioether based-MOFs. The active metal-incorporated MOFs act as an efficient catalyst for a wide range of reactions. The utilization of thiol and thioether MOFs-based catalysts is listed in Table 9.

In 2015, Yee *et al.* post-synthetically modified Zr-DMBD to Zr-DMBD-Hg (Table 9, entry no. 1) by reacting it with an aqueous solution of $HgCl_2$, which was then reacted with H_2O_2

Table 9 Catalysis by thiol-based MOFs

Entry no.	MOFs	Active site	Reaction	Ref.
1	$ZrBDSO_3$-Hg	Hg^{2+} and $-SO_3H$	Acetylene hydration	98
2	Zr-DMBD-I_2	S–I	Iodocyclization of 2-ethynylbenzyl alcohol	99
3	Zr-DMBD-Hg	Hg	Vinylation transfer reaction	102
4	Ag@ Zr-DMBD	Zr, Ag	CO_2 fixation reaction	103
5	UiO-66-PdTCAT	Pd complex	Regioselective C–H oxidation	136
6	UiO-68-$(SH)_2$-Pd	Pd complex	Suzuki–Miyaura reaction (SMR)	67
7	UiO-67-$(SH)_2$-Pd	Pd complex	Suzuki–Miyaura reaction (SMR)	113
8	Pd@UiO–CH_2SO_3H and Pd@UiO–$PHSO_3H$	Pd nanoparticle	Hydrogenolysis of biomass-derived aromatic aldehydes	134
9	Ag@ MOF-s-SH	Cr, Ag	CO_2 fixation reaction	135
10	Ag@UiO-66-SH	Ag nanoparticle	A^3 coupling reaction	141
11	Au^{III} BioMOF and Au^{I} BioMOF	Au^{3+}, Au^{+}	Conversion of alkynes to hydroalkoxylation	92
12	$(Pt^0{}_2)_{0.5}(Pt^{II}Cl_2)$@$[Ca^{II}Cu^{II}_6\{(S,S)$-methox$\}_3(OH)_2(H_2O)]{\cdot}15H_2O$	$Pt^0{}_2$ cluster	CO_2 methanation, alkene hydrogenations, synthesis of HCN and NH_4CN	93
13	$\{Sr^{II}Cu^{II}_6[(S,S)$-serimox$]_{1.50}[(S,S)$-mecysmox$]_{1.50}(OH)_2(H_2O)\}{\cdot}12H_2O$	—	Hemiketalization and ketalization	94

to generate $ZrBDSO_3$-Hg, an effective Lewis acidic heterogeneous catalyst for room-temperature acetylene hydration (Fig. 17a).[98] Interestingly, the catalysis occurred within the pores of the $ZrBDSO_3$-Hg material, which is confirmed by the incapability of the catalyst in relation to larger substrates like 5-propagryloxyisopthalic acids. Wang *et al.* recently reported an exciting result in using the mercury-adsorbed material UiO-66-S-Hg (Table 9, entry no. 3) as a catalyst for vinylation relations, showing good catalytic performance and recyclability (Fig. 17g).[102] The stability of sulfenyl iodides (RS-I) is environment-dependent, making them an interesting family of compounds. In the solution phase, it is precarious for its disproportionation tendency (2RS-I → RSSR + I_2). However, it is stable in a mosaic virus scaffold, and this difference in behaviour inspired the use of a solid support, such as Zr-DMBD, for its unique orientation to synthesize sulfenyl iodides. Solid-supported sulfenyl iodide anchored by Zr-DMBD, abbreviated as Zr-DMBD-I_2, (Table 9, entry no. 2), was synthesized simply by a reaction between Zr-DMBD and I_2.[99] Zr-DMBD-I_2 acts as an efficient heterogeneous catalyst for the iodocyclization of 2-ethynylbenzyl alcohol (Fig. 17b) with a conversion of 93%. Patra *et al.* utilized Zr-DMBD to synthesize a heterogeneous catalyst Ag@Zr-DMBD (Table 9, entry no. 4) by functionalizing the free thiol group of the MOF with an Ag ion and then subsequent reduction to Ag nanoparticles (Fig. 17e). Ag@Zr-DMBD acts as an efficient catalyst with synergistic usage of the Zr and Ag centre for CO_2 fixation by converting the terminal epoxide to corresponding cyclic carbonates in ambient conditions.[103] Ag@MOF-s-SH (Table 9, entry no. 9) synthesized by Liu *et al.* also acts as an efficient catalyst for CO_2 fixation reactions.[135] The Pd metallated MOF UiO-66-PdTCAT synthesized by a PSE strategy from UiO-66 shows heterogeneous catalytic efficiency for the regioselective functionalization of the sp^2 C–H bond (Table 9, entry no. 5).[136] This catalyst is one of the select examples of chelation-assisted C–H functionalization done by a recyclable MOF catalyst. The halogenation of the benzo[h]quinoline with N-chlorosuccinimide (NCS) was performed by the Pd^{2+}-thiocathecolate complexes catalyst (UiO-66-PdTCAT) with 95% of yield and recyclability up to 5 cycles (Fig. 17c). In the thiol-based MOF Zr-DMTD (Table 9, entry no. 6), formed by the expanded linker, the distance between the sulfur atoms of two adjacent ligands in Zr-DMTD is longer than 5.24 Å.[67] The Pd(II) guest forms a covalent link with only one thiol group, freeing up the rest of the coordination sphere for catalysis. The orientation of the thiol groups reduces the thiol's poisoning effect, which is a major problem in solution chemistry. When Pd-loaded Zr-DMTD, namely Zr-DMTD-Pd (S/Pd atom ratio = 2.9 : 1), is examined for the Suzuki Miyaura reaction (SMR) it gives more than 80% yield for iodo substrate (TON > 800) (Fig. 17h). A similar catalytic activity was also observed in the case of lower Pd-loaded samples like Zr-DMTD-Pd (S/Pd atom ratio = 5.2 : 1), from which a conversion rate of 63% was achieved (TON: 1563) with the same reaction conditions [temperature/reaction time (80 °C/8.0 h)]. However, in UiO-67-$(SH)_2$-Pd (Table 9, entry no. 7), the thiol groups of the adjacent ligands are situated near to each other (2.0 Å), and the Pd centre is bonded more exclusively with thiol groups which reduce the catalytic activity.[113] The same reaction conditions for Pd loading as for Zr-TBDD lead to a polycrystalline powder UiO-67-$(SH)_2$-Pd with a S/Pd atom ratio 4.7 : 1 which does not show any catalytic activity in the Suzuki Mayaura reaction; however, with a high temperature of 100 °C the reaction occurs with a conversion rate of 23%. The catalytic activity of the two thiol-based MOFs highlighted the importance of the spatial configuration of the thiol arrays for controlling the coordination environment around the Pd centre.

The post-synthetically synthesized thiol MOF UiO–CH_2SH/UiO–PHSH (Table 9, entry no. 8) is utilized as an efficient catalyst for the hydrogenolysis of biomass-derived aromatic aldehydes (Fig. 17d).[134] Catalyst Pd@UiO–CH_2SO_3H and Pd@UiO–$PHSO_3H$ were synthesized by the incorporation of Pd nanoparticles in UiO–CH_2SO_3H and UiO–$PHSO_3H$ (the oxidized form of UiO–CH_2SH and UiO–PHSH) which was the first report of the integration of an acid site and Pd nanoparticles in MOF cages. The catalyst shows 89.0 and 86.0% DMF yield from MF and HMF and a 99.4% yield of MMP (2-methoxy-4-methylpheno) from lignin-derived VA (vanillin) and shows recyclability up to 4 cycles. Mandal and co-workers have recently utilized silver nanoparticle functionalized thiol MOF Ag@UiO-66-SH as a catalyst for an A^3 type click reaction (Table 9, entry no. 10).[141] The three-component reaction between benzaldehyde, amine and aromatic alkyne leads to the corresponding propargylamine derivatives by C–C bond formation with excellent conversion and recyclability (Fig. 17f). The Ag sites activate the alkyne, which is the rate-determining step of this reaction. Pardo and co-workers extensively work on thioether-based MOFs and their catalytic efficiency.[92–94] The strong affinity of the thioether group was utilized by Mon *et al.* by anchoring a Au salt in BioMOF $\{Ca^{II}Cu^{II}_6[(S,S)\text{-methox}]_3(OH)_2(H_2O)\}\cdot 9H_2O$ to synthesize heterogeneous catalysts Au^{III} BioMOF and Au^{I} BioMOF (Table 9, entry no. 11).[92] Both the catalysts display high efficiency for the conversion of alkynes to the corresponding hydroalkoxylation product (Fig. 17i). Mon *et al.* also utilized these thioether-based MOFs to introduce ultrasmall Pt^0_2 clusters containing heterogenous catalyst $(Pt^0_2)_{0.5}(Pt^{II}Cl_2)$@$[Ca^{II}Cu^{II}_6\{(S,S)\text{-methox}\}_3(OH)_2(H_2O)]\cdot 15H_2O$ which significantly decrease the temperature requirements of some industrially important reactions like CO_2 methanation, alkene hydrogenations, and synthesis of HCN and NH_4CN (Table 9, entry no. 12).[93] Negro *et al.* utilized multivariate (MTV) MOF $\{Sr^{II}Cu^{II}_6[(S,S)\text{-serimox}]_{1.50}[(S,S)\text{-mecysmox}]_{1.50}(OH)_2(H_2O)\}\cdot 12H_2O$ for the hemiketalization of aldehydes and ketalization of (Table 9, entry no. 13) cyclohexanone by mimicking natural nonacidic enzymes.[94]

6.2. Photoswitching and luminescence behaviour

Thiol and thioether-based MOFs display characteristic luminescence behaviour through tuning of the functionalities. Two Pb MOFs synthesized by Xu and co-workers show distinct luminescence behaviour and have only a little difference in their structure with functional changes in the ligand.[123] PbL_{15}

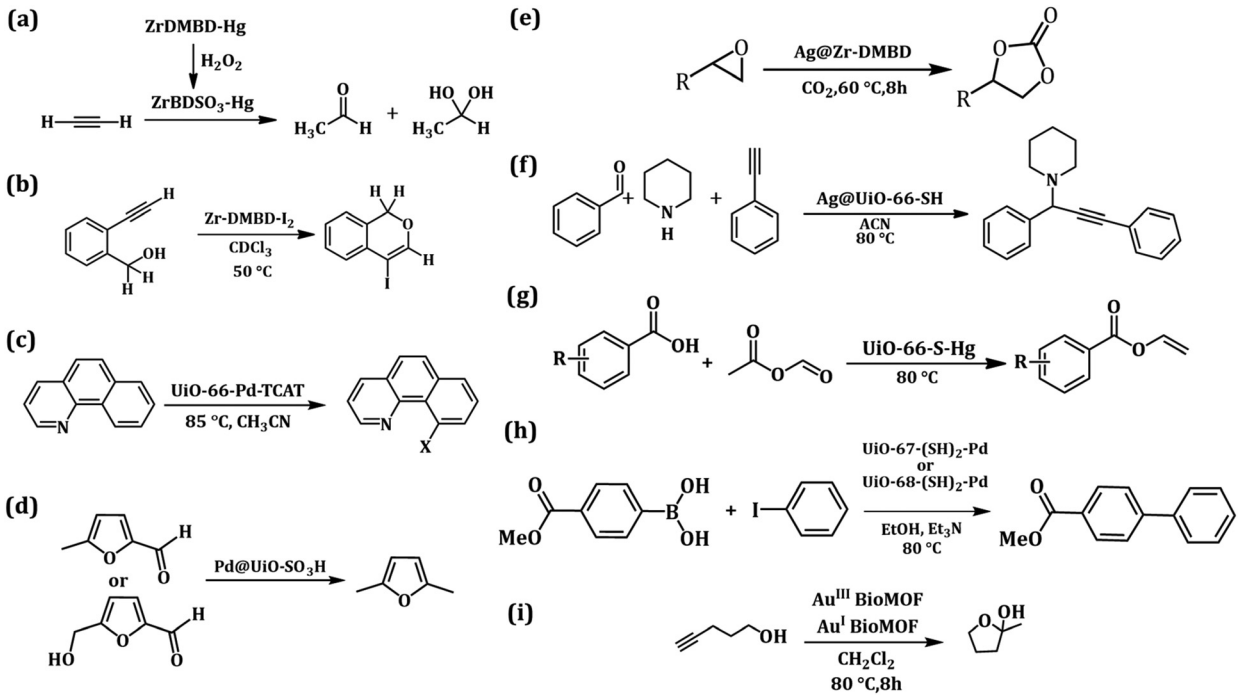

Fig. 17 (a) Acetylene hydration by ZrBDSO$_3$-Hg,[98] (b) iodocyclization of 2-ethynylbenzyl alcohol by Zr-DMBD-I_2,[99] (c) UiO-66-PdTCAT catalyzed C–H activations,[136] (d) hydrogenolysis of biomass-derived aromatic aldehydes,[134] (e) CO_2 fixation reaction by Ag@ Zr-DMBD,[103] (f) Ag@UiO-66-catalysed A^3 coupling reaction,[141] (g) Zr-DMBD-Hg as a vinyl transfer reaction,[102] (h) Suzuki Miyaura reaction (SMR) by Zr-DMTD-Pd and UiO-67-(SH)$_2$-Pd catalyst,[67,113] (i) conversion of alkynes by hydroalkoxylation.[92]

emits bright white light, while PbL_{14} is unable to display white light emission upon exposure to UV radiation. The perturbation caused by the –OH group in the ligand L15 (the structure restricts ligand-to-metal charge transfer (LMCT) and weakens the metal–carboxylate ion interaction in the crystal structure, which stimulates this photophysical changes). The water- and pH-stable thioether-based cadmium MOF reported by Ren and co-workers acts as an efficient luminescence sensor for the detection of heavy metal ions (Cu^{2+}, Hg^{2+}, and Pb^{2+}) from an aqueous medium.[69] Photoinduced electron transfer (PET) between donor–acceptor in the framework generates luminescence activity in the Cd-MOF. The presence of Lewis centres (Cu^{2+}, Hg^{2+}, and Pb^{2+}) inhibits the internal electron transfer which leads to quenching of the emission. Along with the PET mechanism, Förster resonance electron transfer (FRET) (Fig. 18) is also responsible for sensing these heavy metals. Zhou *et al.* reported the colorimetric detection of NH_3 gases using a $[Cu(TMBD)_{0.5}(H_2TMBD)_{0.5}{\cdot}3H_2TMBD]$ structure.[85] The green crystal of the sample becomes blue with exposure to NH_3 gas due to the presence of a stronger ligand field around the Cu^{2+} centres. Zhang and co-workers utilized water-stable Zr-based 2D MOFs (USTS-7) for the selective detection of $Cr^2O_7^{2-}$ with a detection limit of 2.2×10^{-6} mol L^{-1}.[64] Spectroscopic detailed investigation suggests a synergetic effect of the inner filter effect (competitive absorption) and energy transfer phenomena for the selective sensing of dichromate ions. The –OH group in the Zr_6 cluster of USTS-7 shows a strong inclination for dichromate ions and a sizeable overlapping zone between the donor emission (USTS-7) and acceptor absorbance band ($Cr^2O_7^{2-}$) dictates towards the energy transfer mechanism. He *et al.* reported a luminescent thioether linker-mediated MOF which was a prototype of MOF-5 and utilised to detect $HgCl_2$ and nitrobenzene (NB).[122] The blue luminescence of SESMOF-5 diminished after treating with NB vapour and $HgCl_2$ selectively through the inclusion of these molecules into the pores of the framework structure.[122]

A thioether-based linker with alkene functionality induces distinct luminescence properties in ASMOF-5 as reported by Xu and co-workers. The terminal alkene group in the thioether-conjugated aromatic linker potentially activated the interaction between soft metal centres. ASMOF-5 can be used for the selective detect of Pd^{2+} calorimetrically. The orange colour crystal changes into a deep brick red crystal after immersing the compound in an acetonitrile solution of $PdCl_2$.[124] Luo *et al.* recently reported a thiol-functionalized MOF-nanocomposite decorated with PdPt nanoparticles, which exhibits peroxidase (POD) enzymatic activity.[105] Using this POD like activity, a colorimetric detection technique was built up for sensing D-glucose and isomers of chlorophenol.

6.3. Heavy metal adsorptions

The heavy metals mercury (Hg), lead (Pb), arsenic (As), cadmium (Cd) *etc.*, are significant environmental hazards because of their high toxicity.[190] MOFs have been utilized extensively for heavy metal adsorption. Notably, thiol and thioether-based MOFs exhibit significant utility in this domain

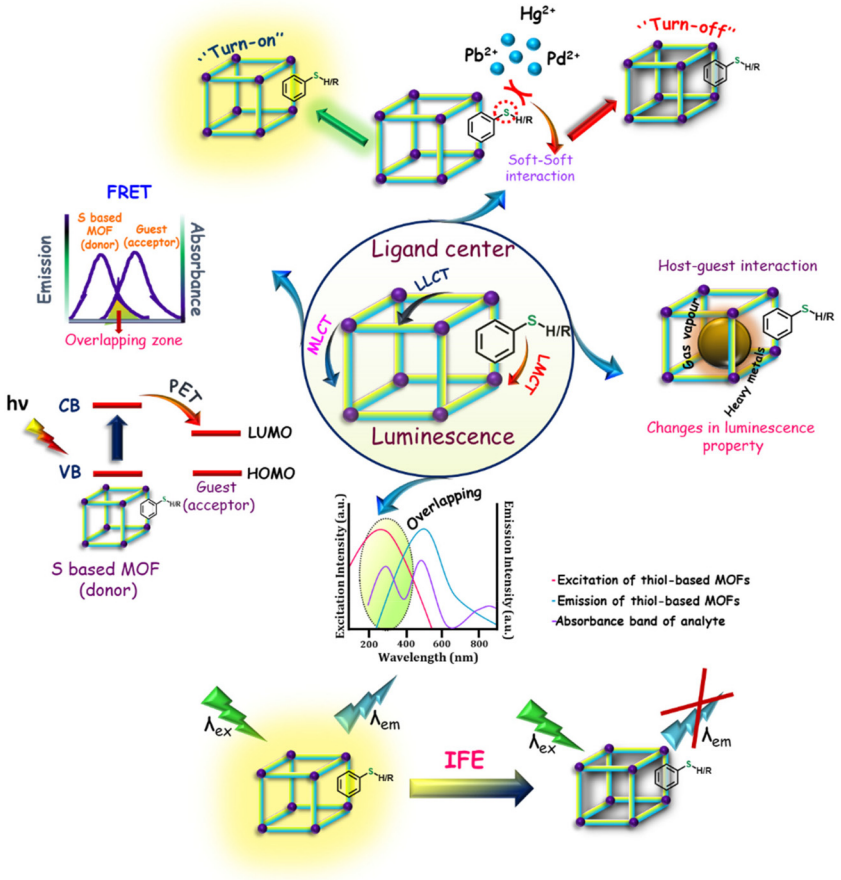

Fig. 18 General sensing mechanism for thiol and thioether-based MOFs.

owing to the existence of electrically soft functional moieties that readily interact with heavy metal species. Li *et al.* have recently provided a comprehensive review of the adsorption capacities of S-based MOFs; thus, we will only give a concise description.[38]

6.3.1 Mercury adsorption. Thiol and thioether-based MOFs have exceptional efficacy in mercury adsorption due to the presence of S-containing functional groups, which possess a high affinity for mercury.[38,191] Mercury exists in highly acidic conditions (pH < 3) as Hg^{2+} and in moderately acidic conditions (3 < pH < 6) as $Hg(OH)^{+}$, but at pH > 6, mercury exists as $Hg(OH)_2$, so pH plays a critical role in the adsorption of mercury.[192] Mercury adsorption by thiol and thioether MOFs is listed in Table 10 and 11, respectively. The first report of Zr-DMBD shows a potential application in Hg^{2+} adsorption in both the solution phase and the gaseous phase (Table 10, entry no. 1).[37] The water-stable Zr-DMBD offers more than 99.9% mercury removal efficiency (Table 10, entry no. 2). Ding *et al.* reported in 2018 an elaborated study of the mechanism of mercury adsorption of Zr-DMBD in different conditions (Table 10, entry no. 3).[193] The maximum capacity for mercury adsorption in Zr-OMPT is 403 mg g^{-1} due to the presence of 8 thiol groups (Table 10, entry no. 4). Since it has incredibly high removal effectiveness, just 10 mg of it can reduce

Table 10 Mercury adsorption by thiol-based MOFs

Entry no.	Thiol-based MOF	Technique used	Adsorption capacity (mg g^{-1})	Removal efficiency	Time (min)	Initial concentration (ppb)	Ref.
1	Zr-DMBD	ICP	—	>99.9%	720	10 000	37
2	Zr-DMBD	AFS	171.5	99.64%	10	10 000	193
3	UiO-66-$(SH)_2$	ICP-MS	236.4	99.9%	1440	10 000	195
4	Zr-OMTP	ICP-MS	403	99.98%	180	6570	114
5	Zr-MSA	ICP-MS	734	99.95%	5	10 000	119
6	Zr-TST	ICP-MS	804	99.5%	2880	6200	117
7	SH-MIL-68(In)	ICP	450.36	>98%	720	10 000	68

Table 11 Mercury adsorption by thioether-based MOFs

Entry no.	Thioether-based MOF	Technique used	Adsorption capacity (mg g^{-1})	Removal efficiency (%)	Time (min)	Initial concentration (ppb)	Ref.
1	PbTMBD	ICP	Hg/Pb 1.06	>79	2880	20	87
2	Zn-MOF	ICP	Zn/Hg 5.56	>94	2880	84 000	122
3	Zr-L_{22}	ICP-AES	275	>96	1200	8000	128
4	Zr-L_{23}	ICP-OES	193	66	1200	10 000	129
5	Zr-L_{24}	ICP-OES	245	>91	1200	8000	129
6	Zr-L_{25}	ICP-OES	322	96	1200	10 000	129
7	MOF-A/S	ICP-AES	9.236	97	—	10 000	184

mercury ion concentrations from 6.57 ppm to 1 ppb. Along with the removal efficiency, Zr-OMPT received special attention because of its high air and boiling water stability. Zr-MSA, synthesized by an aliphatic thiol-based ligand, shows high mercury affinity and adsorbs mercury up to 734 mg g^{-1} (Table 10, entry no. 5).[119]

The primary challenge associated with thiol-based MOFs in mercury adsorption is the high affinity between the thiol group and the mercury ion. This strong interaction poses difficulties during the desorption phase and lowers the recyclability. This issue may be resolved by using thioether-based metal–organic frameworks (MOFs), which enable adsorption and desorption processes to occur at ambient temperature without using strong acids or bases. In the series of thioether-based MOFs reported with ligands L_{22}–L_{25} by He *et al.*, they have explored the influence of sulfide side chains on the framework stability and capacity of mercury adsorption (Table 11, entry no. 3–6).[129] The MOF Zr-L_{25} shows a high adsorption efficiency of 96%. Zr-L_{25} not only adsorbed mercury ions; it also acts as an electrochemical mercury sensor, explored by Fu *et al.* The sensitivity range of the prepared sensor is 0.01 nM to 3 μM, and the detection limit is 7.3 fM.[194] The reversibly bonded Hg^{2+} with the thioether group was regenerated by using 2-mercaptoethanol.

6.3.2 Adsorption of other metal ions. The retrieval of minute quantities of precious metals such as palladium, silver, and gold is essential due to their considerable economic worth and environmental implications. The electronically soft nature of thiol and thioether groups shows strong attraction towards soft noble metals. Thiol and thioether-based MOFs, with their noble metal adsorption capacity, are listed in Table 12.

ASMOF-5 and ASUiO-66 (synthesized from ligand L_{16}) can effectively detect Pd^{2+} in a water medium by a colour change by utilizing the strong interaction between Pd^{2+} and the free-standing alkene group (Table 12, entry no. 1 and 2).[124,125] ASUiO-66 is also an efficient adsorbent for Ag^{+}. UiO-67-$(SH)_2$ can adsorb Pd^{2+}, which can detect the colour change from light yellow to blood red (Table 12, entry no. 3).[113] The post-synthetically synthesized HS-MIL-53(Al) shows a considerable adsorption capacity (182.8 mg g^{-1}) for the Ag^{+} (Table 12, entry no. 4).[133] Thiol-functionalized UiO-66-MAc-50 eq. shows higher adsorption capacity (84 mg g^{-1}) in comparison with its non-functionalized compound UiO-66 (Table 12, entry no. 5).[143] There are some thiol-based MOFs which can adsorb chromium. Cr(VI) adsorption capabilities of 202 and 138.7 mg g^{-1} are shown by Zr-MSA and Zr-DMSA, respectively, efficiently decreasing Cr(VI) by the use of the interaction between the Cr (VI) and thiol groups.[118]

6.3.3 Iodine adsorption. Compared with other functional MOFs, a limited number of thiol and thioether-based MOFs are utilized for iodine adsorption, listed in Table 13. Thiol MOFs CityU-7 and SH-MIL-53(Al) were used for iodine adsorption (Table 13, entry no. 1 and 2). The formation of S–I bonds in MIL-53(Al)-SH shows an adsorption capacity of 325 mg g^{-1} in the equilibrium state.[108] CityU-7 can capture more than 99% of iodine from hexane solution within 6 hours, but the material's recovery is difficult.[86] Thioether-based MOF GDUT-7 (Table 13, entry no. 3) also shows capacity in iodine adsorption.[89]

6.3.4 Dye absorptions. 5-Mercaptoisophthalic acid-containing MOFs $[((CH_3)_2NH_2)Cd(MIPA)]_n{\cdot}xG$ showed high porosity and were tested for dye adsorption, exhibiting selective dye adsorption capacity toward methylene blue (MB).[83] The selective dye adsorptions occur through an ion-exchange mechanism caused by large pore spaces, a high surface area, and the presence of $[(CH_3)_2NH_2]^{+}$ cations in the framework.

6.4. Conductive property

6.4.1 Electrically conductive MOFs. In the history of MOFs, their electronic properties received little attention due to their

Table 12 Noble metal adsorption by thiol and thioether-based MOFs

Entry no.	S-based MOF	Metal ions	Technique used	Adsorption capacity (mg g^{-1})	Ref.
1	ASMOF-5	Pd^{2+}	ICP-OES	—	124
2	ASUiO-66	Pd^{2+}	ICP-AES	45.4	125
3	UiO-67-$(SH)_2$	Pd^{2+}	ICP-OES	—	113
4	HS-MIL-53(Al)	Ag^{+}	ICP-AES	182.8	133
5	UiO-66-MAc	Ag^{+}	AAS	84	143

Table 13 Iodine adsorption by thiol-based MOFs

Entry no.	Thiol and thioether-based MOF	Adsorbate	Technique used	Adsorption capacity (mg g^{-1})	Time (min)	Ref.
1	MIL-53(Al)-SH	I^-	UV/Vis spectroscopy	325	600	108
2	CityU-7	I_2	—	360	86	
3	GDUT-7	I_2	—	120	89	

lower conductivity and they were considered insulators.[196] However, in the last few years, they received recognition after the synthesis and characterization of some electrically conductive MOFs.[197] The electrical conductivity of a material is quantified by the convolution by the charge carrier concentration, n, and the carrier mobility, μ^2. The charge transfer phenomena in conductive MOF generally occur through three pathways: (i) through-bond, (ii) extended conjugation, and (iii) through-space. Thiol or thioether-based MOFs often exhibit conduction *via* a through-bond mechanism. Charge transport may occur *via* continuous coordination or covalent routes known as charge transfer through-bond pathways.[21] The conductive property of some of the thiol-based MOFs was reviewed by Deng *et al.* recently.[39] The MOF-74 family of MOFs have a great contribution in the category of conducting MOFs (formula M_2(DOBDC) where M = divalent metal; DOBDC = 2,5-dioxidobenzene-1,4-dicarboxylate) because it exhibits 1D hexagonal channels and infinite SBUs connecting through $(–M–O)_\infty$ chains, which are responsible for its conductivity.[198,199] Sun *et al.* proposed that if the thiol group can replace the hydroxy group of the linker, it can increase the conductivity of the MOF because of the better energy matching between the frontier orbitals of the metal and the thiolate group.[200] So, the main idea for synthesizing thiol-based MOFs for conductive application is to replace the $(–M–O–)_\infty$ chains to $(–M–S–)_\infty$ for better conductivity. Experimentally it was observed that the framework Mn_2(DSBDC)$(DMF)_2$, where M = divalent metal and DSBDC = 2,5-disulfidobenzene-1,4-dicarboxylate, exhibits a one order higher conductivity (2.5×10^{-12} S cm^{-1}) value than their corresponding oxygen-analogous Mn_2(DOBDC) (3.9×10^{-13} S cm^{-1}) because of the presence of an infinite $(–M–S–)_\infty$ chain (Table 14, entry no. 1 and 2).[109] The conductivity of Fe material (3.9×10^{-6} S cm^{-1}) Fe_2(DSBDC) (Table 14, entry no. 4 and 5) reported by Dincă and co-workers in 2015 is nearly 10^6 times higher than Mn_2(DSBDC) which is also higher than the corresponding oxygen-analogous Fe_2(DOBDC) (3.2×10^{-7} S cm^{-1}).[63] The higher conductivities of Fe material may be due to the loosely bound electrons in the β spin d band of the Fe^{2+}, which decreases the bandgap. Sun *et al.* also studied the effect of DMF in the framework and observed that the guest-free compound shows a little lower conductivity than the as-synthesized material. The defect that originates from the solvent exchange and evacuation process may be the reason for the lowering of conductivity. Eu$(DFDMT)_2$ with a band gap of 1.31 eV shows the conductivity of 4.56×10^{-6} S cm^{-1} due to the presence of a metal-thiolate network with extended π-conjugation (Table 14, entry no. 6).[70] ZrBPD·4F4TS reported by Zhou *et al.* shows a conductivity of 1.1×10^{-5} S cm^{-1} and a band-gap of 2.75 eV. The conductivity increases about 200 times (2.2×10^{-3} S cm^{-1}) in the case of crystalline ZrBPD-4F4TS-Ox (synthesized from ZrBPD-4F4TS by oxidative treatment by $FeCl_3$) because it couples the thiophene units of the MOF (Table 14, entry no. 7) to form a covalent conjugate bridge.[131]

Table 14 The conductivity of different thiol and thioether-based MOFs

Entry no.	Thiol and thioethers based MOF	σ (S cm^{-1})	E_a (eV)	Ref.
1	Mn_2(DSBDC)$(DMF)_2$ solv.	2.5×10^{-12}	—	109
2	Mn_2(DSBDC)$(DMF)_2$ desolv.	1.2×10^{-12}	0.81	
3	Fe_2(DSBDC)$(DMF)_2$ solv.	3.9×10^{-6}	—	63
4	Fe_2(DSBDC)$(DMF)_2$ desolv.	5.8×10^{-7}	0.27	
5	Fe_2(DSBDC) act.	1.5×10^{-9}	—	
6	Eu$(DFDMT)_2$	4.56×10^{-6}	1.31	70
7	ZrBPD·4F4TS-Ox	2.2×10^{-3}	1.66	130
8	$Ni_3(BHT)_2$	0.15		71
9	$Ni_3(BHT)_2$ red.	6.7×10^{-3}		71
10	$Ni_3(BHT)_2$ ox., vac.	160	0.010	162
11	$Ni_3(BHT)_2$ vac.	2.80	0.026	162
12	Ni_3BHT	5	—	166
13	$Pd_3(BHT)_2$	2.8×10^{-2}	—	167
14	Cu-BHT	1580		168
15	Cu_3(BHT)	2500		169
16	Cu_3(BHSe)	110		172
17	Ag_5(BHT)	250	0.0163	163
18	$Ag_3(BHT)_2$	363		173
19	Au_3BHT_2	1.12×10^{-4}		173
20	$Pt_3(THT)_2$	3.86×10^{-4}		72
21	$Fe_3(THT)_2(NH_4)_3$ vac	0.034		175
22	$Fe_3(THT)_2$	0.2		177
23	$Co_3(THT)_2$	1.39×10^{-3}		176
24	Fe_3(PTC)	10		165

$Ni_3(BHT)_2$ exhibits a conductivity value of 0.15 S cm^{-1} in a two-probe pressed pellet, which increases to 2.80 S cm^{-1} for a four-probe pressed pellet (Table 14, entry no. 8–12).[71,162] The presence of a mixed valent charge state (0 and 1) may be the reason for the high conductivity in this material. The oxidised form of the material shows the highest conductivity of 160 S cm^{-1}, whereas the reused form shows the lowest conductivity value of 6.7×10^{-3} S cm^{-1}. Ni_3BHT is nonporous in nature and shows a very small surface area of 25 m^2 g^{-1}, although it showed a high specific capacitance of 245 F g^{-1}, corresponding to a volumetric capacitance of 426 F cm^{-3}, and behaves as a pseudocapacitor, which is very rare for this type of nonporous material.[166] In comparison with $Ni_3(BHT)_2$, $Pd_3(BHT)_2$ shows a relatively lower conductivity of 2.8×10^{-2} S cm^{-1} which may be due to the lower quality of the sample (Table 14, entry no. 13).[167] Cu-BHT shows the highest conductivity (1580 S cm^{-1} at room temperature) among this type of dense (lower porosity)

material (Table 14, entry no. 14).[168] A higher conductivity of 2500 S cm^{-1} was observed for the better crystalline sample as reported by Jin *et. al* (Table 14, entry no. 15).[170] Cu-BHT is the first example of a coordination polymer which could act as a superconductor due to its unique structural density.[170] Huang *et al.* utilized Cu-BHT as an efficient electrocatalyst for the HER.[171] Cu_3(BHSe) also exhibits similar conductivity to Cu-BHT but in thermally activated conditions (Table 14, entry no. 16).[172] The infinite silver–sulfur network containing 2D Ag_5(BHT) shows the conductivity of 250 S cm^{-1}. The charge carrier capacity of this MOF originated from Ag–Ag and Ag–S–Ag chains, which is different from Cu-BHT and Ni-BHT (Table 14, entry no. 17).[163] Ag_3BHT_2 and Au_3BHT_2 are relatively dense in structure and show significant conductivity of 363 S cm^{-1} and 1.12 × 10^{-4} S cm^{-1} (Table 14, entry no. 18 and 19).[173] M-BHT (where M = Co, Ni, Fe) acts as an efficient electrocatalyst for the HER, and the efficiency order is found to be CoBHT > NiBHT > FeBHT.[73]

Thiol-functionalized triphenylene based MOFs are also well known for their significant conductivity. $Pt_3(THT)_2$ shows the conductivity of 3.86 × 10^{-4} S cm^{-1} (Table 14, entry no. 20).[72] Structurally similar $Co_3(THT)_2$ and $Fe_3(THT)_2$ exhibited significant conductivity of 1.4 × 10^{-3} S cm^{-1} and 3.4 × 10^{-2} S cm^{-1} at 300 K (Table 14, entry no. 21).[175,176] $Co_3(THT)_2$ is also an efficient electrocatalyst for the HER whereas $Fe_3(THT)_2$ shows the highest conductivity among this type of material due to band-like charge transportation (Table 14, entry no. 22 and 23).[174] According to Clough *et al.*, while investigating solvent-free $Fe_3(THT)_2$ in the presence of air, the conductivity was further improved, exhibiting metallic behaviour, which can be attributed to the compound's propensity for easy oxidation.[177] Electrocatalyst Co-THT or Ni-THT shows an overpotential of 283 mV and 315 mV with the Tafel slope of 71 and 76 mV dec^{-1} in 0.5 M H_2SO_4 solution.[178] $Ni_3(THT)_2$ acts as an efficient electrocatalyst, which shows the overpotential of 333 mV and a Tafel slope of 80.5 dec^{-1} in 0.5 M H_2SO_4 solution.[179] In acidic conditions (pH = 1.3) the MOFs $[Co_3(BHT)_2]^{3-}$ and $[Co_3(THT)_2]^{3-}$ show an overpotential of 0.34 V and 0.53 V at 10 mA cm^{-2}, respectively, for the HER reaction.[174] The mechanism involves protonation of the sulfur sites on the dithiolene ligands subsequent to the first reduction of Co^{3+}/Co^{2+}. Perthiolated coronene-based MOF Fe_3(PTC) shows conductivity up to 10 S cm^{-1} at temperatures below 20 K; the observed phenomenon can be attributed to the hybridization of d and p orbitals originating from iron (Fe), the coronene core, and the iron-sulfur Fe-S_4 nodes (Table 14, entry no. 24).[165] Co-PTC shows a conductivity of 45 S cm^{-1} and acts as an excellent HER catalyst whereas Ni-PTC exhibits a conductivity of 10 S cm^{-1}.[180,181] The benzene-1,2,4,5-tetrathiolate (BTT)-containing thiol MOF NiBT exhibits an overpotential of 470 mV at pH = 1.3 with a current density of 10 mA cm^{-2}.[164]

Thiol MOF-based composite CC@UiO-66$(SH)_2$ combined with a Li–S battery exhibits a better discharge capacity of 1209 mA h g^{-1} at 0.1 C, outstanding cyclic stability, and high efficiency.[150] Recently, Mandal and co-workers reported the HER activity (hydrogen evolution reaction) of Au and Ag nanoparticle immobilized thiol NU-1000-SH.[138,139] The composite material Au@NU-1000-SH exhibits an overpotential of 101 mV at a current density of 10 mA cm^{-2} with a Tafel slope of 44 mV dec^{-1}. The control experiment explains the importance of specific thiol MOF and Au nanoparticle interaction in the HER experiment, which shows cycling stability up to 36 h.[139] Ag@NU-1000-SH demonstrated an overpotential of 165 mV at a current density of 10 mA cm^{-2} with a Tafel slope of 53 mA dec^{-1}.[138] Mandal and co-workers have also synthesized Ag@UiO-66-SH and utilized it as an efficient electrocatalytic catalyst for carbon dioxide reduction.[142] The silver nanoparticle-incorporated catalyst shows a mass activity of 218 A g^{-1} with a faradaic efficiency (FE) of 74% and a high partial current density of 19.5 mA cm^{-2} at −1.2 V for CO. Recently Li *et al.* utilized Ag@Zr-DMBD to to achieve reversible stripping, which shows a specific capacity of 159.8 mA h g^{-1}.[107]

6.5. Proton conductivity

In recent years proton exchange membrane fuel cells (PEMFCs) have received enormous attention because of their efficient energy conversions and nearly zero emission.[201] Popular PEMFCs contain terminal sulfonic acid groups, which help with high proton conductivity in humid conditions.[202] Polysulfones, polybenzimidazoles, polyimides, and polyaryl ether ketones are some of the alternative materials being investigated for use in PEMFCs; however, the aromatic-based polymers need functionalization with a sulfonic acid group to provide effective proton conductivity.[203] The construction of PEMFC membranes using MOFs is important because of the tunable pore surface and the regularity of the void space in the structure. The proton conductivity of a substance is a measure of its proton mobility. One method to boost proton mobility is to include guest molecules in the MOF structure, such as triazole or imidazole ammonium cations or hydronium ions. These encased molecules create a proton conduction route by hydrogen bonding with water molecules already present in the lattice. The alternative strategy takes advantage of an acidic organic moiety since the pK_a values of the functional group determine the proton conductivity.[204] The commercially available, highly efficient PEMFC Nafion contains sulfonic acid groups in terminal positions. So, researchers tried to install the sulfonic acid groups in the MOF for high conductivity. The direct interaction between a sulfonic acid-containing ligand and a metal ion to introduce a non-coordinating sulfonic acid group in a metal–organic framework (MOF) is not a favourable approach due to the tendency of the sulfonic acid group to coordinate with metal ions. Due to these difficulties, post-synthetic modifications of MOFs containing suitable functional groups received attention.[205] Easily oxidizable thiol and thioether-group-containing MOFs are advantageous in this category. Thiol and thioether-based MOFs reported for proton conductivity are listed in Table 15.

Water-stable Zr-DMBD, which contains a free-standing thiol group, is suitable for the post-synthetic incorporation of a sulfonic acid group to increase the charge carrier density. Phang

Table 15 Proton conductivity of different MOFs

Entry no.	MOFs	Conductivity σ/S cm^{-1}	E_a/eV	Ref.
1	UiO-66$(SO_3H)_2$	8.4×10^{-2} (80 °C, 90% RH)	0.32	97
2	Zr-BPDC-4SO_2Me4F	1.75×10^{-4} (80 °C, 90% RH)	—	130
3	ZrBPD-4F4TS	6.0×10^{-5} (80 °C, 90% RH)	2.75	131
4	ZrBPD-4F4TS-Ox	5.0×10^{-7} (80 °C, 90% RH)	1.66	131
5	ZrTST	9.2×10^{-4} (80 °C, 90% RH)	0.97	117
6	ZrTSaT	0.37 (90 °C, 90% RH)	1.18	117

et al. reported UiO-66$(SO_3H)_2$ with the simple oxidation of Zr-DMBD by H_2O_2 (Table 15, entry no. 1).[97] The H_2O present in the pores of the MOF is easily converted to H_3O^+ by the easily donated proton from $-SO_3H$ and shows a long-term proton conductivity of 8.4×10^{-2} S cm^{-1} at 80 °C (90% relative humidity). The boiling water-stable thioether-based Zr-BPDC-4S4F (Table 15, entry no. 2) synthesized by Xian *et al.* shows high proton conductivity when its thiol group is oxidized to the sulfonic acid group by a similar strategy.[130] Zr-BPDC-4SO_2Me4F is the oxidized form of Zr-BPDC-4S4F and shows proton conductivity of 1.75×10^{-4} S cm^{-1} at 80 °C (90% relative humidity), which is a thousand times more than the precursor Zr-BPDC-4S4F (Fig. 19). The Zr MOF ZrBPD-4F4TS (Table 15, entry no. 3 and 4) synthesized by He and co-workers reported in 2021 shows proton conductivity of 6.0×10^{-5} S cm^{-1} at 80 °C (90% RH).[131]

ZrBPD-4F4TS is not acid-stable, so treating it with acid was impossible for better proton conductivity. When acid-stable ZrBPD-4F4TS-Ox is examined for proton conductivity, it shows a lower proton conductivity of 5.0×10^{-7} S cm^{-1} at 90% RH and 80 °C, which is due to the rigidity of the framework, but when it is treated with dilute sulfuric acid, the proton conductivity increases a thousand times (1.6×10^{-3} S cm^{-1} at 90% RH and 80 °C).

The recently reported MOF ZrTST (Table 15, entry no. 5) by He *et al.* shows proton conductivity of 9.2×10^{-4} S cm^{-1} (80 °C, 90% relative humidity), which is 37 times more than well-known thiol-based MOF Zr-DMBD (2.5×10^{-5} S cm^{-1} at 80 °C, 90% RH). The m-CPBA oxidized form of ZrTST is highly stable ZrTSaT (Table 15, entry no. 6) and shows excellent proton conductivity of 0.22 S cm^{-1} at 80 °C and 90% RH and 0.37 S cm^{-1} at 90 °C and 90% RH.

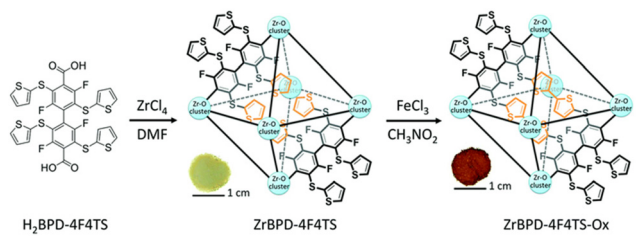

Fig. 19 Synthesis of ZrBPD-4F4TS-Ox.[131] (Adapted with permission from the Royal Society of Chemistry.)

6.6. Photocatalytic property

Recent studies have shown MOFs as a novel class of photocatalysts that can degrade different materials under light irradiation.[23] The facile synthesis of MOFs is facilitated by the availability of many metal-containing nodes and organic functionalized linkers.[206] Different organic functional group-containing ligands like –OH, –SH, $-NO_2$, and $-NH_2$ are more capable of narrowing the band gap of the MOF, which leads to a bathochromic shift of the spectrum.[207] Some thiol and thioether-containing MOFs show efficient photocatalytic activity for H_2 evolution, CO_2 reduction and pollutant degradations.[100,116,137,151]

6.6.1 Photocatalyst for H_2 evolution reaction. Thiol and thioether-based MOFs, which are efficient photocatalysts for HER, are listed in Table 16. Chen *et al.* studied the visible-light-driven photocatalytic property of the three isoreticular MOFs with S-functionality UiO-66-$(SO_3H)_2$, UiO-66-$(SH)_2$ and UiO-66-$(SCH_3)_2$.[100] Pt nanoparticles are used as a co-catalyst as noble metal nanoparticles act as an electron reservoir. Between these three MOFs, Pt/UiO-66-$(SCH_3)_2$ shows (Table 16, entry no. 1) the highest efficiency for photocatalytic H_2 generation (3871 μmol g^{-1}) from water with sacrificial ascorbic acid (0.2 M) under $\lambda > 400$ nm irradiation (Fig. 20a). Metalloporphyrin compounds are well known for their diverse photophysical properties, like strong absorbance in the UV region, outstanding photosensitizing ability, and feasible functionalization by peripheral substitution or metal ion complexations. These photophysical properties of metalloporphyrins make porphyrin-grafted MOFs an efficient photocatalyst (Fig. 20b).[116] Generally, when metalloporphyrins are excited by photons, they create electrons and holes. The positive holes are quenched immediately by a sacrificial electron donor (triethanolamine), and the excited electrons migrate to the Pt co-catalyst, which leads to the reduction of H^+ on Pt to generate hydrogen gases.

Pristine ZrTTA-6SH (Table 16, entry no. 2), when tested for its photocatalytic applications, exhibits a minimal capacity for H_2 evolution, but when the pristine MOF is grafted with different metal porphyrins (*i.e.*, Zn, Ni, Fe), it enhances its photocatalytic activity. Metalloporphyrin (MTFPP) guest also acts as a robust anchor of the photocatalyst, preventing the catalyst's leaching and increasing recyclability. UiO-66-DCBDT-M (M = Fe, Ni, Cu) synthesized by Zhong *et al.*[112] were examined for the photocatalytic H_2 evolution reaction, where UiO-66-DCBDT-Cu shows the best result. The noble metal free hetero-

Table 16 Photocatalysis activity of thiol and thioether-based MOFs for the H_2 evolution reaction

Entry no.	Photocatalyst	Light source	Scavenger	H_2 evolution (mmol h^{-1} g^{-1})	Ref.
1	Pt/UiO-66-$(SCH_3)_2$	(λ > 400 nm) xenon lamp	Ascorbic acid	3871	100
2	Porphyrin grafted ZrTTA-6SH	(λ > 400 nm)	TEOA	110	116
3	UiO-66-DCBDT-Cu@TiO_2	300 W xenon lamp	TEOA	12.63	112
4	Pt/20%-MIL-125-$(SCH_3)_2$	(λ > 400 nm) xenon lamp	TEOA	3814	137
5	SCu-CZS	225 W xenon lamp	TEOA	42.55	149
6	Ni_2P/UIOS	($\lambda \geq$ 420 nm) xenon lamp	Ascorbic acid	3724	151

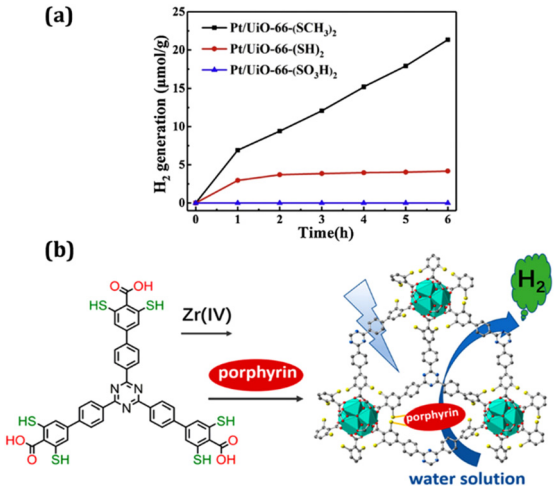

Fig. 20 (a) At room temperature, the time course of H_2 production of Pt/UiO-66-X_2 from aqueous solution with 0.1 vol% TEOA as an electronic sacrificial reagent.[100] (b) Schematic diagram of photocatalysis by porphyrine-grafted ZrTTA-6SH.[116] (Adapted with permission from Elsevier Inc and the American Chemical Society.)

junction UiO-66-DCBDT-Cu@TiO_2 shows the HER rate of 12.63 mmol g^{-1} h^{-1} (Table 16, entry no. 3). The –SCH_3 group containing *X*%-MIL-125-$(SCH_3)_2$ (where *X* is 20% and 50%) reported by Han *et al.* shows high photocatalytic activity for H_2 production in the presence of Pt co-catalyst (Table 16, entry no. 4). It was found that 20%-MIL-125-$(SCH_3)_2$ shows the highest efficiency for H_2 production 3814 μmol g^{-1} h^{-1} in comparison with other well-established amino-functionalized MIL-125.[137] This report indicates the importance of the thioether group containing MOFs as a photocatalyst. Ni_2P nanoparticle-incorporated thioether-based composite shows an excellent photocatalytic H_2 evolution efficiency of 3724 mmol h^{-1} g^{-1}, which is 187 times the corresponding UIOS MOF. Moreover, the composite outperforms the previously published UIOS catalyst using Pt nanoparticles (Table 16, entry no. 6).[151]

6.6.2 Photocatalysts for CO_2 reduction. CO_2 is a highly stable linear molecule with fully oxidized carbon, which makes the reduction of CO_2 unfavourable. Visible light-driven photocatalyst plays a vital role in CO_2 reduction.[208] Cobalt anchored Zr-DMBD, abbreviated as Zr-DMBD-Co(II), is an efficient catalyst for visible-light-driven CO_2-to-CO conversion with high selectivity.[101] A series of Zr-DMBD-Co-*x* (*x* is the weight percentage of Co(II) ions 0.002 to 0.2%) was synthesized by reacting with different concentrations of $CoCl_2$ solution to obtain the photocatalytic activity of the Zr-DMBD-Co, and from the experiment, it is observed that Zr-DMBD-Co-0.002% shows the highest TON (97 941) in a water-containing system.

6.6.3 Catalytic reduction of Cr(VI). Cr(VI) is a water-soluble, highly toxic element that has a range of detrimental effects on living organisms.[209] Reducing Cr(VI) to less soluble Cr(III) is a helpful strategy to address this problem. Compared with the chemical approach, the photocatalytic reduction of Cr(VI) has garnered interest due to its high efficiency, cheap cost, and environmental friendliness. Some thiol-based MOFs are efficient as a photocatalyst for Cr(VI) reductions, like SH-UiO-66(Zr)/Pd, which shows very high efficiency in photocatalytic Cr(VI) reduction.[140]

6.6.4 Photocatalytic dye degradation. Organic dyes can act as pollutants, particularly when they are released into the environment without proper treatment. Recently the photocatalytic degradation of organic dyes received considerable attention because of their cost efficiency and sustainability.

The Ag nanoparticle composite (Ag@MOF-s-SH) of the mesoporous MOF NH_2-MIL-101(Cr)-s can photocatalytically degrade RhB dye efficiently.[135]

6.7 Gas adsorption

Runčevski *et al.* reported Mn_2(DSBDC) containing coordinatively unsaturated Mn^{2+} centres, which promotes the adsorption of multiple gas molecules simultaneously.[110] Generally, maximum gas-adsorbing MOFs are capable only of adsorbing a single gas molecule, which limits the storage capacity of the MOFs, but activated Mn_2(DSBDC) can adsorb two gas molecules, such as D_2, CD_4 and CO_2, at a time. The reason behind this capability of the MOF is the structure where two Mn are present with two different coordinate environments. In the structure, six atoms from the DSBDC linker connected with Mn(1) and in Mn(2), four atoms from DSBDC linker and two DMF molecules with a *cis* arrangement connected to form two different kinds of octahedral centre. It is hypothesized that if a metal centre contains more than one terminal solvent molecule, the activated material containing an unsaturated low coordinating metal centre can effectively accommodate more gas molecules.

In the case of CPM-8S, the surface area is surprisingly lower than in ZIF-8, but it shows a high adsorption of 107 cm^3 g^{-1} for CO_2, which is much higher than ZIF-8 (29 cm^3 g^{-1}).[76] CPM-8S can separate light hydrocarbons like C_2H_6, C_2H_4 and

C_2H_2. Triphenylenehexathiol-containing MOFs with Co, Ni, and Cu were examined for the electrochemically controlled reversible capture and release of ethylene.[210] It was observed that the application of a positive potential (+2.0 V) promoted ethylene capture, and by applying a negative potential of (−2.0 V), the gases could be released, which was quantified by NMR.

7. Concluding remarks and future perspectives

In recent years, there has been significant interest in thiol and thioether-based MOFs due to their distinctive advantages, *viz.* a combination of both hard and soft functional groups, high stability, and wide-ranging applications, including catalysis, sensing, gas adsorption, conductivity, and heavy metal adsorption. Despite the benefits of thiol and thioether-based MOFs, it is essential to highlight related challenges like the following. (i) Synthetic difficulties: due to the limited accessibility of thiol and thioether-based ligands, a perpetual shortage of these ligands persists. In the majority of instances, the synthesis of ligands involves a series of sequential reactions that require inert conditions and anhydrous solvents. This requirement renders the synthesis process both laborious and costly. The propensity to oxidation of thiol and thioether groups also creates difficulties for synthesizing thiol and thioether-based MOFs. (ii) Difficulties in structure determinations: as many thiol and thioether-based MOFs are powder in nature, it creates difficulties in analyzing the structures. (iii) Strong interaction with heavy metals: many thiol-based MOFs act as an adsorbent, so strong interactions between the S and heavy metals make reversible processes difficult and make the adsorbent less efficient by slowing the desorption process. (iv) Practical applications: maximum reported thiol and thioether-based MOFs are far from their industrial application and only prove the concept.

Despite the difficulties of thiol and thioether-based MOFs, a decent number of MOFs of this family were synthesized, characterized, and utilized for catalysis, sensing, heavy metal adsorption, conductivity, and other applications. Regardless of the explorations of thiol and thioether-based MOFs from the last 15 years, there is always the opportunity for synthesizing new thiol and thioether-based ligands by organic transformations, which will lead to corresponding thiol and thioether-based MOFs. Post-synthetic modifications are vast, so there is always scope for synthesizing new thiol and thioether-based MOFs from well-established MOFs with different functionalities. Many directions are yet to venture, like synthesizing different thiol and thioether-based MOFs containing other functional groups, which may bring an exciting property to the MOF. There is also the opportunity to synthesize different MOFs from thiol and thioether-based MOFs, like thiol oxidation to sulfonic acid groups, thiol groups to other thioether chains, *etc.*

Considering the potential and difficulties that lie ahead, we think this particular class of MOFs has a diverse and exciting future. In this perspective, we have summarized all the aspects of the bi-functional thiol and thioether-based MOFs like synthetic approaches where two major classes of synthetic approach, *i.e.* synthesis from thiol and thioether-based ligands and synthesis by indirect methods, along with structural differences, has been discussed. Thiol and thioether-based MOFs show applications in a wide range of areas.

In conclusion, thiol and thioether-based MOFs represent a fascinating and rapidly evolving area of research in functional materials. Their unique properties, structural versatility, and diverse applications underscore their potential impact across heavy metal adsorption, sensing, catalysis, gas adsorption and conductivity. As researchers continue to push the boundaries of MOF science, it is clear that thiol and thioether-based MOFs will continue to captivate our attention and contribute to scientific advancements in the years to come.

We believe this perspective will help the researcher understand the area of thiol and thioether-based MOFs precisely. We want to highlight Dr. Zhengtao Xu's contribution (**https://orcid.org/0000-0002-7408-4951**) for his substantial contributions in this area (thiol and thioether-based MOFs). We sincerely apologize for missing any significant results.

Abbreviations

1D	One dimensional
2D	Two dimensional
3D	Three dimensional
ACN	Acetonitrile
BET	Brunauer–Emmett–Teller
DMF	Dimethylformamide
DMSO	Dimethyl sulphoxide
HSAB	Hard–soft-acid–base
ICP-OES	Inductively coupled plasma optical emission spectrometry
LOD	Limit of detection
m-CPBA	*meta*-Chloroperoxybenzoic acid
MIL	Material of Institute Lavoisier
MOF	Metal–organic framework
MS	Mass spectrometry
Np	Nanoparticle
NU	North Western University
PXRD	Powder X-ray diffraction
SBU	Secondary building units
SC-XRD	Single crystal X-ray diffraction
SEM	Scanning electron microscope
TEM	Transmission electron microscope
UiO	University of Oslo

Conflicts of interest

There is no conflict to declare.

Acknowledgements

The authors thank IIT Patna for resources. The Science and Engineering Research Board, DST, Govt. of India, is acknowledged for a research grant under sanction ECR/2018/001306.

References

1 O. M. Yaghi, M. O'Keeffe, N. W. Ockwig, H. K. Chae, M. Eddaoudi and J. Kim, *Nature*, 2003, **423**, 705–714.
2 H. Furukawa, K. E. Cordova, M. O'Keeffe and O. M. Yaghi, *Science*, 2013, **341**, 1230444.
3 H. C. Zhou, J. R. Long and O. M. Yaghi, *Chem. Rev.*, 2012, **112**, 673–674.
4 N. Stock and S. Biswas, *Chem. Rev.*, 2012, **112**, 933–969.
5 H. Li, M. Eddaoudi, M. O'Keeffe and O. M. Yaghi, *Nature*, 1999, **402**, 276–279.
6 C. Jiang, X. Wang, Y. Ouyang, K. Lu, W. Jiang, H. Xu, X. Wei, Z. Wang, F. Dai and D. Sun, *Nanoscale Adv.*, 2022, **4**, 2077–2089.
7 A. Pal, S. Chand and M. C. Das, *Inorg. Chem.*, 2017, **56**, 13991–13997.
8 P. A. Kobielska, A. J. Howarth, O. K. Farha and S. Nayak, *Coord. Chem. Rev.*, 2018, **358**, 92–107.
9 G. K. Dam, S. Fajal, S. Dutta, S. Let, A. V. Desai and S. K. Ghosh, *ACS Appl. Opt. Mater.*, 2023, **1**, 1217–1226.
10 T. A. Goetjen, J. Liu, Y. Wu, J. Sui, X. Zhang, J. T. Hupp and O. K. Farha, *Chem. Commun.*, 2020, **56**, 10409–10418.
11 A. Bavykina, N. Kolobov, I. S. Khan, J. A. Bau, A. Ramirez and J. Gascon, *Chem. Rev.*, 2020, **120**, 8468–8535.
12 A. Gogia and S. K. Mandal, *ACS Appl. Mater. Interfaces*, 2022, **14**, 27941–27954.
13 R. Das and C. M. Nagaraja, *Green Chem.*, 2021, **23**, 5195–5204.
14 U. Patel, P. Patel, B. Parmar, A. Dadhania and E. Suresh, *Cryst. Growth Des.*, 2021, **21**, 1833–1842.
15 P. P. Mondal, N. Seal, M. Singh and S. Neogi, *Dalton Trans.*, 2023, **52**, 8661–8669.
16 S. Sahoo, S. Mondal and D. Sarma, *Coord. Chem. Rev.*, 2022, **470**, 214707.
17 L. E. Kreno, K. Leong, O. K. Farha, M. Allendorf, R. P. Van Duyne and J. T. Hupp, *Chem. Rev.*, 2012, **112**, 1105–1125.
18 T. Kumar, M. Venkateswarulu, B. Das, A. Halder and R. R. Koner, *Dalton Trans.*, 2019, **48**, 12382–12385.
19 S. Mallakpour, E. Nikkhoo and C. M. Hussain, *Coord. Chem. Rev.*, 2022, **451**, 214262.
20 Z. Zhou, M. Vázquez-González and I. Willner, *Chem. Soc. Rev.*, 2021, **50**, 4541–4563.
21 L. S. Xie, G. Skorupskii and M. Dincă, *Chem. Rev.*, 2020, **120**, 8536–8580.
22 D.-W. Lim and H. Kitagawa, *Chem. Rev.*, 2020, **120**, 8416–8467.
23 Q. Wang, Q. Gao, A. M. Al-Enizi, A. Nafady and S. Ma, *Inorg. Chem. Front.*, 2020, **7**, 300–339.
24 G. Mínguez Espallargas and E. Coronado, *Chem. Soc. Rev.*, 2018, **47**, 533–557.
25 S. Biswas, A. K. Mondal and S. Konar, *Inorg. Chem.*, 2016, **55**, 2085–2090.
26 Y. Shen, A. Tissot and C. Serre, *Chem. Sci.*, 2022, **13**, 13978–14007.
27 X. Li, R. Anderson, H. C. Fry, S. M. Pratik, W. Xu, S. Goswami, T. G. Allen, J. Yu, S. S. Rajasree, C. J. Cramer, G. Rumbles, D. A. Gómez-Gualdrón and P. Deria, *ACS Appl. Mater. Interfaces*, 2023, **15**, 28228–28239.
28 M. Ding, X. Cai and H.-L. Jiang, *Chem. Sci.*, 2019, **10**, 10209–10230.
29 O. K. Farha, I. Eryazici, N. C. Jeong, B. G. Hauser, C. E. Wilmer, A. A. Sarjeant, R. Q. Snurr, S. T. Nguyen, A. Ö. Yazaydın and J. T. Hupp, *J. Am. Chem. Soc.*, 2012, **134**, 15016–15021.
30 X. Zhang, Z. Chen, X. Liu, S. L. Hanna, X. Wang, R. Taheri-Ledari, A. Maleki, P. Li and O. K. Farha, *Chem. Soc. Rev.*, 2020, **49**, 7406–7427.
31 W. Lu, Z. Wei, Z.-Y. Gu, T.-F. Liu, J. Park, J. Park, J. Tian, M. Zhang, Q. Zhang, T. Gentle Iii, M. Bosch and H.-C. Zhou, *Chem. Soc. Rev.*, 2014, **43**, 5561–5593.
32 Y. Lin, C. Kong and L. Chen, *RSC Adv.*, 2016, **6**, 32598–32614.
33 S. Cadot, L. Veyre, D. Luneau, D. Farrusseng and E. Alessandra Quadrelli, *J. Mater. Chem. A*, 2014, **2**, 17757–17763.
34 Z. Feng, J. Yang, L. Zhu and T. Sun, *Colloids Surf., A*, 2023, **658**, 130701.
35 A. Schneemann, Y. Jing, J. D. Evans, T. Toyao, Y. Hijikata, Y. Kamiya, K.-i. Shimizu, N. C. Burtch and S.-i. Noro, *Dalton Trans.*, 2021, **50**, 10423–10435.
36 J. He, S. Cheng and Z. Xu, *Chem. – Eur. J.*, 2019, **25**, 8654–8662.
37 K.-K. Yee, N. Reimer, J. Liu, S.-Y. Cheng, S.-M. Yiu, J. Weber, N. Stock and Z. Xu, *J. Am. Chem. Soc.*, 2013, **135**, 7795–7798.
38 X. Li, W. Ma, H. Li, Q. Zhang and H. Liu, *Coord. Chem. Rev.*, 2020, **408**, 213191.
39 X. Deng, S.-L. Zheng, Y.-H. Zhong, J. Hu, L.-H. Chung and J. He, *Coord. Chem. Rev.*, 2022, **450**, 214235.
40 Y.-A. Li, C.-W. Zhao, N.-X. Zhu, Q.-K. Liu, G.-J. Chen, J.-B. Liu, X.-D. Zhao, J.-P. Ma, S. Zhang and Y.-B. Dong, *Chem. Commun.*, 2015, **51**, 17672–17675.
41 S. Kunath, M. Schindeldecker, A. De Giacomo, T. Meyer, S. Sohre, P. Hajieva, C. von Schacky, J. Urban and B. Moosmann, *Redox Biol.*, 2020, **36**, 101628.
42 M. A. Comini, *Free Radic. Res.*, 2016, **50**, 246–271.
43 G. J. Beckett and J. D. Hayes, *Adv. Clin. Chem.*, 1993, **30**, 281–380.
44 C. Gaucher, A. Boudier, J. Bonetti, I. Clarot, P. Leroy and M. Parent, *Antioxid. Act.*, 2018, **7**, 62.
45 A. Ghorbani-Choghamarani, M. Nikoorazm, H. Goudarziafshar and B. Tahmasbi, *Chem. Inf.*, 2009, **40**, i.
46 L. Wang, L. Liu and H. Zhao, *Angew. Chem., Int. Ed.*, 2023, **62**, e202304073.

47 C. Dai, H. Zhang, R. Li and H. Zou, *Pol. J. Chem. Technol.*, 2019, **21**, 35–39.
48 B. H. Northrop and R. N. Coffey, *J. Am. Chem. Soc.*, 2012, **134**, 13804–13817.
49 J. Du, L. Chen, X. Zeng, S. Yu, W. Zhou, L. Tan, L. Dong, C. Zhou and J. Cheng, *ACS Appl. Mater. Interfaces*, 2020, **12**, 28576–28585.
50 A. V. Davis and T. V. O'Halloran, *Nat. Chem. Biol.*, 2008, **4**, 148–151.
51 M. V. Trivedi, J. S. Laurence and T. J. Siahaan, *Curr. Protein Pept. Sci.*, 2009, **10**, 614–625.
52 M. Platen and E. Steckhan, *Liebigs Ann. Chem.*, 1984, **1984**, 1563–1576.
53 S. G. Murray and F. R. Hartley, *Chem. Rev.*, 1981, **81**, 365–414.
54 R. E. Hansen and J. R. Winther, *Anal. Biochem.*, 2009, **394**, 147–158.
55 D. J. C. Prasad and G. Sekar, *Org. Lett.*, 2011, **13**, 1008–1011.
56 H. Chen, W. Jiang and Q. Zeng, *Chem. Rec.*, 2020, **20**, 1269–1296.
57 B. Xiong, V. Jha, J.-K. Min and J. Cho, *Exp. Mol. Med.*, 2020, **52**, 390–399.
58 J. T. Jarrett, *J. Biol. Chem.*, 2015, **290**, 3972–3979.
59 K. Konstas, T. Osl, Y. Yang, M. Batten, N. Burke, A. J. Hill and M. R. Hill, *J. Mater. Chem. A*, 2012, **22**, 16698–16708.
60 Z.-J. Wang, L.-J. Han, X.-J. Gao and H.-G. Zheng, *norg. Chem.*, 2018, **57**, 5232–5239.
61 D. Sarma, K. V. Ramanujachary, N. Stock and S. Natarajan, *Cryst. Growth Des.*, 2011, **11**, 1357–1369.
62 Y. Wang, L.-J. Zhang, R. Zhang, Y. Jin, Y. Wang, Y.-H. Xing, F.-Y. Bai and L.-X. Sun, *Cryst. Growth Des.*, 2017, **17**, 6531–6540.
63 L. Sun, C. H. Hendon, M. A. Minier, A. Walsh and M. Dincă, *J. Am. Chem. Soc.*, 2015, **137**, 6164–6167.
64 J. Liu, S. Liu, J. Ma, Y. Diao, M. Li, J. He, S. Chen and Q. Zhang, *Inorg. Chem.*, 2020, **59**, 17884–17888.
65 J. He, C. Yang, Z. Xu, M. Zeller, A. D. Hunter and J. Lin, *J. Solid State Chem.*, 2009, **182**, 1821–1826.
66 L. Fu, S. Wang, G. Lin, L. Zhang, Q. Liu, J. Fang, C. Wei and G. Liu, *J. Hazard. Mater.*, 2019, **368**, 42–51.
67 B. Gui, K.-K. Yee, Y.-L. Wong, S.-M. Yiu, M. Zeller, C. Wang and Z. Xu, *Chem. Commun.*, 2015, **51**, 6917–6920.
68 G.-P. Li, K. Zhang, P.-F. Zhang, W.-N. Liu, W.-Q. Tong, L. Hou and Y.-Y. Wang, *Inorg. Chem.*, 2019, **58**, 3409–3415.
69 B. Mohan, Z. Tao, S. Kumar, T. Xing, S. Ma, W. Huang, X. Yang, H. You and P. Ren, *Cryst. Growth Des.*, 2022, **22**, 5407–5415.
70 Q. Zeng, L. Wang, Y. Huang, S.-L. Zheng, Y. He, J. He, W.-M. Liao, G. Xu, M. Zeller and Z. Xu, *Chem. Commun.*, 2020, **56**, 3645–3648.
71 T. Kambe, R. Sakamoto, K. Hoshiko, K. Takada, M. Miyachi, J.-H. Ryu, S. Sasaki, J. Kim, K. Nakazato and M. Takata, *J. Am. Chem. Soc.*, 2013, **135**, 2462–2465.
72 J. Cui and Z. Xu, *Chem. Commun.*, 2014, **50**, 3986–3988.
73 C. A. Downes, A. J. Clough, K. Chen, J. W. Yoo and S. C. Marinescu, *ACS Appl. Mater. Interfaces*, 2018, **10**, 1719–1727.
74 H. Yang, X. Zhang, G. Zhang and H. Fei, *Chem. Commun.*, 2018, **54**, 4469–4472.
75 X.-Y. Yang, S. Yuan, J.-S. Qin, C. Lollar, A. Alsalme and H.-C. Zhou, *Mater. Chem. Front.*, 2017, **1**, 1764–1767.
76 Y. Gai, X. Chen, H. Yang, Y. Wang, X. Bu and P. Feng, *Chem. Commun.*, 2018, **54**, 12109–12112.
77 J. Winarta, B. Shan, S. M. McIntyre, L. Ye, C. Wang, J. Liu and B. Mu, *Cryst. Growth Des.*, 2020, **20**, 1347–1362.
78 S. Øien-Ødegaard, B. Bouchevreau, K. Hylland, L. Wu, R. Blom, C. Grande, U. Olsbye, M. Tilset and K. P. Lillerud, *Inorg. Chem.*, 2016, **55**, 1986–1991.
79 F. Millange, C. Serre and G. Férey, *Chem. Commun.*, 2002, 822–823.
80 S. Rojas-Buzo, B. Bohigues, C. W. Lopes, D. M. Meira, M. Boronat, M. Moliner and A. Corma, *Chem. Sci.*, 2021, **12**, 10106–10115.
81 M. Kim and S. M. Cohen, *CrystEngComm*, 2012, **14**, 4096–4104.
82 T. Ahnfeldt, D. Gunzelmann, T. Loiseau, D. Hirsemann, J. Senker, G. Férey and N. Stock, *Inorg. Chem.*, 2009, **48**, 3057–3064.
83 B.-X. Dong, M. Tang, W.-L. Liu, Y.-C. Wu, Y.-M. Pan, F.-Y. Bu and Y.-L. Teng, *Cryst. Growth Des.*, 2016, **16**, 6363–6370.
84 X.-P. Zhou, Z. Xu, M. Zeller, A. D. Hunter, S. S.-Y. Chui and C.-M. Che, *Inorg. Chem.*, 2008, **47**, 7459–7461.
85 X.-P. Zhou, Z. Xu, J. He, M. Zeller, A. D. Hunter, R. Clérac, C. Mathonière, S. S.-Y. Chui and C.-M. Che, *Inorg. Chem.*, 2010, **49**, 10191–10198.
86 J. Liu, R. Xiao, Y.-L. Wong, X.-P. Zhou, M. Zeller, A. D. Hunter, Q. Fang, L. Liao and Z. Xu, *Inorg. Chem.*, 2018, **57**, 4807–4811.
87 X.-P. Zhou, Z. Xu, M. Zeller and A. D. Hunter, *Chem. Commun.*, 2009, 5439–5441.
88 X.-P. Zhou, Z. Xu, M. Zeller, A. D. Hunter, S. S.-Y. Chui, C.-M. Che and J. Lin, *Inorg. Chem.*, 2010, **49**, 7629–7631.
89 Y. He, M. Huang, X. Deng, C. Shengxian, Y.-L. Wong, Y.-L. Hou, J. He, M. Zeller and Z. Xu, *Chem. Commun.*, 2019, **55**, 5091–5094.
90 J. Cui, Y.-L. Wong, M. Zeller, A. D. Hunter and Z. Xu, *Angew. Chem., Int. Ed.*, 2014, **53**, 14438–14442.
91 M. Mon, X. Qu, J. Ferrando-Soria, I. Pellicer-Carreño, A. Sepúlveda-Escribano, E. V. Ramos-Fernandez, J. C. Jansen, D. Armentano and E. Pardo, *J. Mater. Chem. A*, 2017, **5**, 20120–20125.
92 M. Mon, J. Ferrando-Soria, T. Grancha, F. R. Fortea-Pérez, J. Gascon, A. Leyva-Pérez, D. Armentano and E. Pardo, *J. Am. Chem. Soc.*, 2016, **138**, 7864–7867.
93 M. Mon, M. A. Rivero-Crespo, J. Ferrando-Soria, A. Vidal-Moya, M. Boronat, A. Leyva-Pérez, A. Corma, J. C. Hernández-Garrido, M. López-Haro and J. J. Calvino, *Angew. Chem.*, 2018, **130**, 6294–6299.

94 C. Negro, S. Sanz-Navarro, A. Leyva-Pérez, D. Armentano, J. Ferrando-Soria and E. Pardo, *Inorg. Chem.*, 2023, **62**, 7353–7359.
95 J. H. Cavka, S. Jakobsen, U. Olsbye, N. Guillou, C. Lamberti, S. Bordiga and K. P. Lillerud, *J. Am. Chem. Soc.*, 2008, **130**, 13850–13851.
96 G. Wißmann, A. Schaate, S. Lilienthal, I. Bremer, A. M. Schneider and P. Behrens, *Microporous Mesoporous Mater.*, 2012, **152**, 64–70.
97 W. J. Phang, H. Jo, W. R. Lee, J. H. Song, K. Yoo, B. Kim and C. S. Hong, *Angew. Chem., Int. Ed.*, 2015, **54**, 5142–5146.
98 K.-K. Yee, Y.-L. Wong, M. Zha, R. Y. Adhikari, M. T. Tuominen, J. He and Z. Xu, *Chem. Commun.*, 2015, **51**, 10941–10944.
99 K.-K. Yee, Y.-L. Wong and Z. Xu, *Dalton Trans.*, 2016, **45**, 5334–5338.
100 T.-F. Chen, S.-Y. Han, Z.-P. Wang, H. Gao, L.-Y. Wang, Y.-H. Deng, C.-Q. Wan, Y. Tian, Q. Wang, G. Wang and G.-S. Li, *Appl. Catal., B*, 2019, **259**, 118047.
101 D.-C. Liu, T. Ouyang, R. Xiao, W.-J. Liu, D.-C. Zhong, Z. Xu and T.-B. Lu, *ChemSusChem*, 2019, **12**, 2166–2170.
102 Y. Wang, X. Zhu, X. Zhang, J. Zheng, H. Li, N. Xie, Y. Guo, H.-b. Sun and G. Zhang, *Dalton Trans.*, 2022, **51**, 4043–4051.
103 R. Patra and D. Sarma, *Dalton Trans.*, 2023, **52**, 10795–10804.
104 Y. Luo, X. Zhao, Z. Gao, H. Wang, Y. Liu, C. Guo and Y. Pan, *Anal. Chim. Acta*, 2022, **1202**, 339665.
105 Y. Luo, S. Zhou, W. Chen, Y. Liu, H. Feng and Y. Pan, *J. Mater. Chem. B*, 2023, **11**, 6634–6645.
106 S. Chowdhury, P. Sharma, K. Kundu, P. P. Das, P. Rathi and P. F. Siril, *Inorg. Chem.*, 2023, **62**, 3875–3885.
107 X. Li, Y. Su, Y. Qin, F. Huang, S. Mei, Y. He, C. Peng, L. Ding, Y. Zhang, Y. Peng and Z. Deng, *Adv. Mater.*, 2023, 2303489.
108 A. S. Munn, F. Millange, M. Frigoli, N. Guillou, C. Falaise, V. Stevenson, C. Volkringer, T. Loiseau, G. Cibin and R. I. Walton, *CrystEngComm*, 2016, **18**, 8108–8114.
109 L. Sun, T. Miyakai, S. Seki and M. Dincă, *J. Am. Chem. Soc.*, 2013, **135**, 8185–8188.
110 T. Runčevski, M. T. Kapelewski, R. M. Torres-Gavosto, J. D. Tarver, C. M. Brown and J. R. Long, *Chem. Commun.*, 2016, **52**, 8251–8254.
111 H. Yang, F. Peng, C. Dang, Y. Wang, D. Hu, X. Zhao, P. Feng and X. Bu, *J. Am. Chem. Soc.*, 2019, **141**, 9808–9812.
112 H. Zhong, S. Chen, Z. Jiang, J. Hu, J. Dong, L.-H. Chung, Q.-C. Lin, W. Ou, L. Yu and J. He, *Small*, 2023, **19**, 2207266.
113 Y.-L. Wong, Y. Diao, J. He, M. Zeller and Z. Xu, *Inorg. Chem.*, 2019, **58**, 1462–1468.
114 M.-Q. Li, Y.-L. Wong, T.-S. Lum, K. Sze-Yin Leung, P. K. S. Lam and Z. Xu, *J. Mater. Chem. A*, 2018, **6**, 14566–14570.
115 S. Wu, Z. Li, M.-Q. Li, Y. Diao, F. Lin, T. Liu, J. Zhang, P. Tieu, W. Gao, F. Qi, X. Pan, Z. Xu, Z. Zhu and A. K. Y. Jen, *Nat. Nanotechnol.*, 2020, **15**, 934–940.
116 Y. Diao, N. Xu, M.-Q. Li, X. Zhu and Z. Xu, *Inorg. Chem.*, 2020, **59**, 12643–12649.
117 Y. He, J. Dong, Z. Liu, M.-Q. Li, J. Hu, Y. Zhou, Z. Xu and J. He, *ACS Appl. Mater. Interfaces*, 2022, **14**, 1070–1076.
118 P. Yang, Y. Shu, Q. Zhuang, Y. Li and J. Gu, *Langmuir*, 2019, **35**, 16226–16233.
119 P. Yang, Y. Shu, Q. Zhuang, Y. Li and J. Gu, *Chem. Commun.*, 2019, **55**, 12972–12975.
120 J. Ma, A. G. Wong-Foy and A. J. Matzger, *Inorg. Chem.*, 2015, **54**, 4591–4593.
121 H. Furukawa, F. Gándara, Y.-B. Zhang, J. Jiang, W. L. Queen, M. R. Hudson and O. M. Yaghi, *J. Am. Chem. Soc.*, 2014, **136**, 4369–4381.
122 J. He, K.-K. Yee, Z. Xu, M. Zeller, A. D. Hunter, S. S.-Y. Chui and C.-M. Che, *Chem. Mater.*, 2011, **23**, 2940–2947.
123 J. He, M. Zeller, A. D. Hunter and Z. Xu, *J. Am. Chem. Soc.*, 2012, **134**, 1553–1559.
124 J. He, M. Zha, J. Cui, M. Zeller, A. D. Hunter, S.-M. Yiu, S.-T. Lee and Z. Xu, *J. Am. Chem. Soc.*, 2013, **135**, 7807–7810.
125 M. Zha, J. Liu, Y.-L. Wong and Z. Xu, *J. Mater. Chem. A*, 2015, **3**, 3928–3934.
126 Y.-L. Wong, K.-K. Yee, Y.-L. Hou, J. Li, Z. Wang, M. Zeller, A. D. Hunter and Z. Xu, *Inorg. Chem.*, 2018, **57**, 6198–6201.
127 A. D. Burrows, C. G. Frost, M. F. Mahon and C. Richardson, *Chem. Commun.*, 2009, 4218–4220.
128 Y.-L. Hou, K.-K. Yee, Y.-L. Wong, M. Zha, J. He, M. Zeller, A. D. Hunter, K. Yang and Z. Xu, *J. Am. Chem. Soc.*, 2016, **138**, 14852–14855.
129 Y. He, Y.-L. Hou, Y.-L. Wong, R. Xiao, M.-Q. Li, Z. Hao, J. Huang, L. Wang, M. Zeller, J. He and Z. Xu, *J. Mater. Chem.*, 2018, **6**, 1648–1654.
130 W.-R. Xian, Y. He, Y. Diao, Y.-L. Wong, H.-Q. Zhou, S.-L. Zheng, W.-M. Liao, Z. Xu and J. He, *Inorg. Chem.*, 2020, **59**, 7097–7102.
131 H.-Q. Zhou, Y. He, J.-Y. Hu, L.-H. Chung, Q. Gu, W.-M. Liao, M. Zeller, Z. Xu and J. He, *Chem. Commun.*, 2021, **57**, 187–190.
132 S. Mandal, S. Natarajan, P. Mani and A. Pankajakshan, *Adv. Funct. Mater.*, 2021, **31**, 2006291.
133 X. Cheng, M. Liu, A. Zhang, S. Hu, C. Song, G. Zhang and X. Guo, *Nanoscale*, 2015, **7**, 9738–9745.
134 Q. Deng, J. Zhu, Y. Zhong, X. Li, J. Wang, J. Cai, Z. Zeng, J.-J. Zou and S. Deng, *ACS Sustainable Chem. Eng.*, 2021, **9**, 11127–11136.
135 X. Liu, C. Hu, J. Wu, H. Zhu, Y. Li, P. Cui and F. Wei, *J. Solid State Chem.*, 2021, **296**, 121889.
136 H. Fei and S. M. Cohen, *J. Am. Chem. Soc.*, 2015, **137**, 2191–2194.
137 S.-Y. Han, D.-L. Pan, H. Chen, X.-B. Bu, Y.-X. Gao, H. Gao, Y. Tian, G.-S. Li, G. Wang, S.-L. Cao, C.-Q. Wan and G.-C. Guo, *Angew. Chem., Int. Ed.*, 2018, **57**, 9864–9869.
138 S. Muhamed, R. K. Aparna, A. Karmakar, S. Kundu and S. Mandal, *Nanoscale*, 2022, **14**, 17345–17353.

139 S. Muhamed, R. K. Aparna, A. Karmakar, S. Kundu and S. Mandal, *Inorg. Chem.*, 2023, **62**, 7195–7202.
140 A. Pankajakshan, A. Ravarikkandy, B. P. Ratheesh, M. P. Maman and S. Mandal, *Inorg. Chem. Front.*, 2021, **8**, 5093–5099.
141 R. K. Aparna, S. Mukherjee, S. S. Rose and S. Mandal, *Inorg. Chem.*, 2022, **61**, 16441–16447.
142 R. K. Aparna, V. Surendran, D. Roy, B. Pathak, M. M. Shaijumon and S. Mandal, *ACS Appl. Energy Mater.*, 2023, **6**, 4072–4078.
143 B. Moll, T. Müller, C. Schlüsener, A. Schmitz, P. Brandt, S. Öztürk and C. Janiak, *Mater. Adv.*, 2021, **2**, 804–812.
144 Q.-L. Zhu and Q. Xu, *Chem. Soc. Rev.*, 2014, **43**, 5468–5512.
145 H. Yang, C. Peng, J. Han, Y. Song and L. Wang, *Sens. Actuators, B*, 2020, **320**, 128447.
146 S. Gholizadeh Khasevani and M. R. Gholami, *Mater. Res. Bull.*, 2018, **106**, 93–102.
147 J. Chen, F. Chao, X. Mu, J. Jiang, Q. Zhu, J. Ren, Y. Guo and Y. Lou, *Inorg. Chem. Commun.*, 2019, **102**, 25–29.
148 G. Boix, J. Troyano, L. Garzón-Tovar, C. Camur, N. Bermejo, A. Yazdi, J. Piella, N. G. Bastus, V. F. Puntes, I. Imaz and D. Maspoch, *ACS Appl. Mater. Interfaces*, 2020, **12**, 10554–10562.
149 S. Mao, J.-W. Shi, G. Sun, Y. Zhang, X. Ji, Y. Lv, B. Wang, Y. Xu and Y. Cheng, *Chem. Eng. J.*, 2021, **404**, 126533.
150 X. Hu, S. Lin, R. Chen, G. Zhang, T. Huang, J. Li, X. Yang, L.-H. Chung, L. Yu and J. He, *ACS Appl. Mater. Interfaces*, 2022, **14**, 31942–31950.
151 X. Li, Q. Li, T. Zhang, Y. Lou and J. Chen, *Dalton Trans.*, 2022, **51**, 12282–12289.
152 D. C. Fox, A. T. Fiedler, H. L. Halfen, T. C. Brunold and J. A. Halfen, *J. Am. Chem. Soc.*, 2004, **126**, 7627–7638.
153 E. I. Solomon, S. I. Gorelsky and A. Dey, *J. Comput. Chem.*, 2006, **27**, 1415–1428.
154 P. Venkateswara Rao and R. H. Holm, *Chem. Rev.*, 2004, **104**, 527–560.
155 L. Rizzi, A. Zienert, J. Schuster, M. Köhne and S. E. Schulz, *ACS Appl. Mater. Interfaces*, 2018, **10**, 43088–43094.
156 G. Bian, J. Yin and J. Zhu, *Small*, 2021, **17**, 2006043.
157 L. Cao and C. Wang, *ACS Cent. Sci.*, 2020, **6**, 2149–2158.
158 M. Tawalbeh, H. A. Khan and A. Al-Othman, *J. Energy Storage*, 2023, **60**, 106656.
159 V. Orts Mercadillo, K. C. Chan, M. Caironi, A. Athanassiou, I. A. Kinloch, M. Bissett and P. Cataldi, *Adv. Funct. Mater.*, 2022, **32**, 2204772.
160 Y. Guo, K. Wang, Y. Hong, H. Wu and Q. Zhang, *Dalton Trans.*, 2021, **50**, 11331–11346.
161 T. Chen, J.-H. Dou, L. Yang, C. Sun, N. J. Libretto, G. Skorupskii, J. T. Miller and M. Dincă, *J. Am. Chem. Soc.*, 2020, **142**, 12367–12373.
162 T. Kambe, R. Sakamoto, T. Kusamoto, T. Pal, N. Fukui, K. Hoshiko, T. Shimojima, Z. Wang, T. Hirahara and K. Ishizaka, *J. Am. Chem. Soc.*, 2014, **136**, 14357–14360.
163 X. Huang, H. Li, Z. Tu, L. Liu, X. Wu, J. Chen, Y. Liang, Y. Zou, Y. Yi and J. Sun, *J. Am. Chem. Soc.*, 2018, **140**, 15153–15156.
164 R. Matsuoka, R. Sakamoto, T. Kambe, K. Takada, T. Kusamoto and H. Nishihara, *Chem. Commun.*, 2014, **50**, 8137–8139.
165 R. Dong, Z. Zhang, D. C. Tranca, S. Zhou, M. Wang, P. Adler, Z. Liao, F. Liu, Y. Sun and W. Shi, *Nat. Commun.*, 2018, **9**, 2637.
166 H. Banda, J.-H. Dou, T. Chen, N. J. Libretto, M. Chaudhary, G. M. Bernard, J. T. Miller, V. K. Michaelis and M. Dincă, *J. Am. Chem. Soc.*, 2021, **143**, 2285–2292.
167 T. Pal, T. Kambe, T. Kusamoto, M. L. Foo, R. Matsuoka, R. Sakamoto and H. Nishihara, *ChemPlusChem*, 2015, **80**, 1255–1258.
168 X. Huang, P. Sheng, Z. Tu, F. Zhang, J. Wang, H. Geng, Y. Zou, C.-a. Di, Y. Yi and Y. Sun, *Nat. Commun.*, 2015, **6**, 7408.
169 Z. Jin, J. Yan, X. Huang, W. Xu, S. Yang, D. Zhu and J. Wang, *Nano Energy*, 2017, **40**, 376–381.
170 X. Huang, S. Zhang, L. Liu, L. Yu, G. Chen, W. Xu and D. Zhu, *Angew. Chem.*, 2018, **130**, 152–156.
171 X. Huang, H. Yao, Y. Cui, W. Hao, J. Zhu, W. Xu and D. Zhu, *ACS Appl. Mater. Interfaces*, 2017, **9**, 40752–40759.
172 Y. Cui, J. Yan, Z. Chen, J. Zhang, Y. Zou, Y. Sun, W. Xu and D. Zhu, *Adv. Sci.*, 2019, **6**, 1802235.
173 I.-F. Chen, C.-F. Lu and W.-F. Su, *Langmuir*, 2018, **34**, 15754–15762.
174 A. J. Clough, J. W. Yoo, M. H. Mecklenburg and S. C. Marinescu, *J. Am. Chem. Soc.*, 2015, **137**, 118–121.
175 R. Dong, P. Han, H. Arora, M. Ballabio, M. Karakus, Z. Zhang, C. Shekhar, P. Adler, P. S. Petkov and A. Erbe, *Nat. Mater.*, 2018, **17**, 1027–1032.
176 A. J. Clough, J. M. Skelton, C. A. Downes, A. A. de la Rosa, J. W. Yoo, A. Walsh, B. C. Melot and S. C. Marinescu, *J. Am. Chem. Soc.*, 2017, **139**, 10863–10867.
177 A. J. Clough, N. M. Orchanian, J. M. Skelton, A. J. Neer, S. A. Howard, C. A. Downes, L. F. J. Piper, A. Walsh, B. C. Melot and S. C. Marinescu, *J. Am. Chem. Soc.*, 2019, **141**, 16323–16330.
178 R. Dong, Z. Zheng, D. C. Tranca, J. Zhang, N. Chandrasekhar, S. Liu, X. Zhuang, G. Seifert and X. Feng, *Chem. – Eur. J.*, 2017, **23**, 2255–2260.
179 R. Dong, M. Pfeffermann, H. Liang, Z. Zheng, X. Zhu, J. Zhang and X. Feng, *Angew. Chem., Int. Ed.*, 2015, **54**, 12058–12063.
180 Z. Chen, Y. Cui, C. Ye, L. Liu, X. Wu, Y. Sun, W. Xu and D. Zhu, *Chem. – Eur. J.*, 2020, **26**, 12868–12873.
181 Z. Chen, Y. Cui, Y. Jin, L. Liu, J. Yan, Y. Sun, Y. Zou, Y. Sun, W. Xu and D. Zhu, *J. Mater. Chem. C*, 2020, **8**, 8199–8205.
182 C. A. Downes and S. C. Marinescu, *Dalton Trans.*, 2016, **45**, 19311–19321.
183 C. A. Downes and S. C. Marinescu, *J. Am. Chem. Soc.*, 2015, **137**, 13740–13743.
184 G.-W. Xiao, T.-F. Chen, X.-Z. Sun, H. Guo, Z.-F. Li, Y.-H. Deng and C.-Q. Wan, *Dalton Trans.*, 2017, **46**, 12036–12040.

185 C. Pettinari, A. Tăbăcaru and S. Galli, *Coord. Chem. Rev.*, 2016, **307**, 1–31.
186 V. Colombo, C. Montoro, A. Maspero, G. Palmisano, N. Masciocchi, S. Galli, E. Barea and J. A. R. Navarro, *J. Am. Chem. Soc.*, 2012, **134**, 12830–12843.
187 J. Hu, X. Deng, H. Zhang, Y. Diao, S. Cheng, S.-L. Zheng, W.-M. Liao, J. He and Z. Xu, *Inorg. Chem.*, 2021, **60**, 161–166.
188 V. Pascanu, G. González Miera, A. K. Inge and B. Martín-Matute, *J. Am. Chem. Soc.*, 2019, **141**, 7223–7234.
189 M. Mukoyoshi and H. Kitagawa, *Chem. Commun.*, 2022, **58**, 10757–10767.
190 G. Pandey and S. Madhuri, *Res. J. Anim. Vet. Fish. Sci.*, 2014, **2**, 17–23.
191 X. Yan, P. Li, X. Song, J. Li, B. Ren, S. Gao and R. Cao, *Coord. Chem. Rev.*, 2021, **443**, 214034.
192 Y. Yin, H. E. Allen, Y. Li, C. P. Huang and P. F. Sanders, *J. Environ. Qual.*, 1996, **25**, 837–844.
193 L. Ding, X. Luo, P. Shao, J. Yang and D. Sun, *ACS Sustainable Chem. Eng.*, 2018, **6**, 8494–8502.
194 L. Fu, K. Xie, A. Wang, F. Lyu, J. Ge, L. Zhang, H. Zhang, W. Su, Y.-L. Hou, C. Zhou, C. Wang and S. Ruan, *Anal. Chim. Acta*, 2019, **1081**, 51–58.
195 K. Leus, J. P. H. Perez, K. Folens, M. Meledina, G. Van Tendeloo, G. Du Laing and P. Van Der Voort, *Faraday Discuss.*, 2017, **201**, 145–161.
196 L. Sun, M. G. Campbell and M. Dincă, *Angew. Chem., Int. Ed.*, 2016, **55**, 3566–3579.
197 C. Li, L. Zhang, J. Chen, X. Li, J. Sun, J. Zhu, X. Wang and Y. Fu, *Nanoscale*, 2021, **13**, 485–509.
198 W. Zhou, H. Wu and T. Yildirim, *J. Am. Chem. Soc.*, 2008, **130**, 15268–15269.
199 P. I. Scheurle, A. Mähringer, A. C. Jakowetz, P. Hosseini, A. F. Richter, G. Wittstock, D. D. Medina and T. Bein, *Nanoscale*, 2019, **11**, 20949–20955.
200 L. Sun, C. H. Hendon, S. S. Park, Y. Tulchinsky, R. Wan, F. Wang, A. Walsh and M. Dincă, *Chem. Sci.*, 2017, **8**, 4450–4457.
201 N. Delaporte, E. Rivard, S. K. Natarajan, P. Benard, M. L. Trudeau and K. Zaghib, *Nanomaterials*, 2020, **10**, 1947.
202 W. J. Phang, H. Jo, W. R. Lee, J. H. Song, K. Yoo, B. Kim and C. S. Hong, *Angew. Chem.*, 2015, **127**, 5231–5235.
203 D. J. Jones and J. Rozière, *J. Membr. Sci.*, 2001, **185**, 41–58.
204 A. Shigematsu, T. Yamada and H. Kitagawa, *J. Am. Chem. Soc.*, 2011, **133**, 2034–2036.
205 K. K. Tanabe and S. M. Cohen, *Angew. Chem., Int. Ed.*, 2009, **48**, 7424–7427.
206 A. Dhakshinamoorthy, Z. Li and H. Garcia, *Chem. Soc. Rev.*, 2018, **47**, 8134–8172.
207 K. Hendrickx, D. E. P. Vanpoucke, K. Leus, K. Lejaeghere, A. Van Yperen-De Deyne, V. Van Speybroeck, P. Van Der Voort and K. Hemelsoet, *Inorg. Chem.*, 2015, **54**, 10701–10710.
208 C. I. Ezugwu, S. Liu, C. Li, S. Zhuiykov, S. Roy and F. Verpoort, *Coord. Chem. Rev.*, 2022, **450**, 214245.
209 M. Tumolo, V. Ancona, D. De Paola, D. Losacco, C. Campanale, C. Massarelli and V. F. Uricchio, *Int. J. Environ. Res.*, 2020, **17**, 5438.
210 L. Mendecki, M. Ko, X. Zhang, Z. Meng and K. A. Mirica, *J. Am. Chem. Soc.*, 2017, **139**, 17229–17232.